CHALMERS

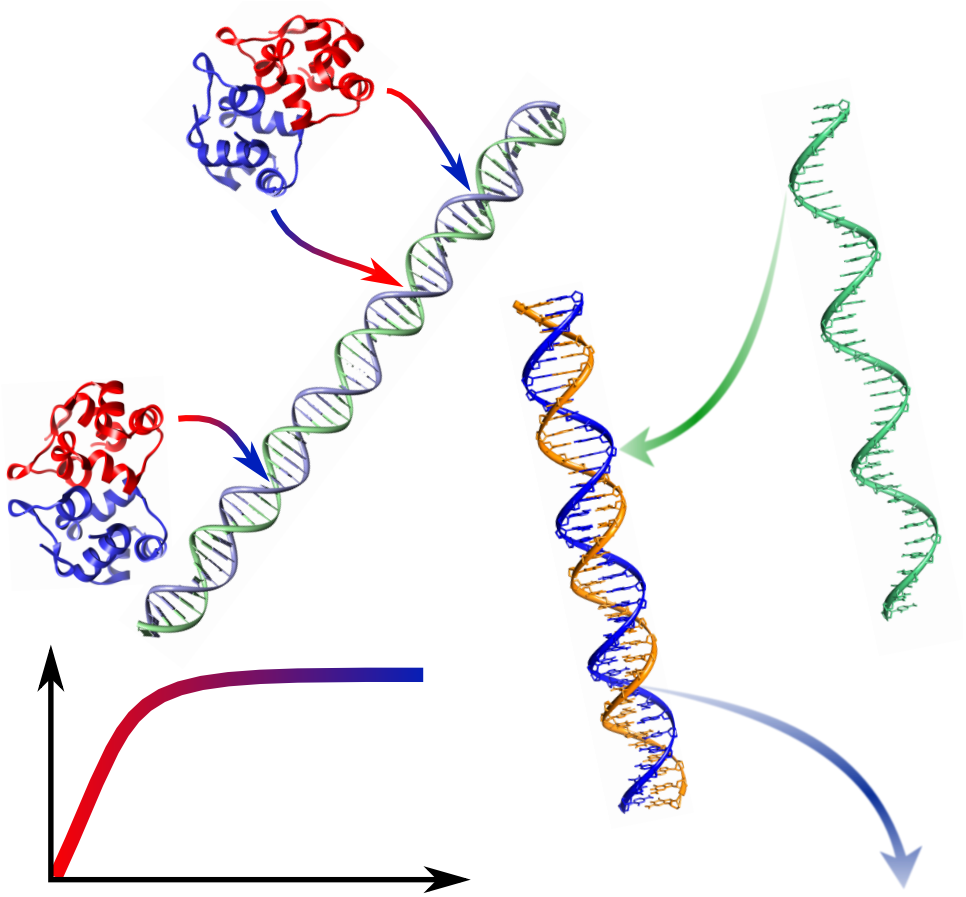

Studying DNA Strand Exchange and Binding of a Repressor Protein using Fluorescent Base Analogues

Master of Science Thseis

Damir Džebo

Department of Chemical and Biological Engineering
Division of Chemistry and Biochemistry, Physical Chemistry
CHALMERS UNIVERSITY OF TECHNOLOGY
Göteborg, Sweden, 2011

THESIS FOR THE DEGREE OF MASTER OF SCIENCES

Studying DNA Strand Exchange and Binding of a Repressor Protein using Fluorescent Base Analogues

Damir Džebo

CHALMERS

Department of Chemical and Biological Engineering
CHALMERS UNIVERSITY OF TECHNOLOGY
Gothenburg, Sweeden, 2011

Studying DNA Strand Exchange and Binding of a Repressor Protein using Fluorescent Base Analogues

Damir Džebo

Department of Chemical and Biological Engineering
Chalmers University of Technology
SE-412 96 Göteborg
Sweden
Telephone: +46 (0)31 772 10 10

Cover picture:
Left: two P2 C repressor proteins binding to a DNA duplex containing operators with a cartoon of the binding curve below. *Right:* a schematic illustration of DNA strand exchange with strands of same length and sequence as those used in this Thesis.

Department of Chemical and Biological Engineering
Göteborg, Sweden 2011

Studying DNA Strand Exchange and Binding of a Repressor Protein using Fluorescent Base Analogues

Damir Džebo

Department of Chemical and Biological Engineering
Chalmers University of Technology

ABSTRACT

Strand exchange between double- and single-stranded DNA is similar in all cell-based organisms, where it plays a key role in both DNA repair and genetic diversity. In life, this reaction is catalyzed by recombination enzymes but the underlying mechanisms are not yet fully understood. In this thesis, the pure reaction without recombination enzymes is studied using the fluorescent base analogue tC^O and by utilizing a synthetic crowding environment created using different forms of polyethylene glycol (PEG). All forms of PEG used accelerated the DNA strand exchange compared to the same reaction in buffer. A low molecular weight PEG, PEG178, significantly accelerated the process and gave an inverse rate constant (τ) of 71.04 s.

The protein P2 C repressor regulates the immune response towards the P2 virus in *Escherichia coli*. In this thesis, the binding of the P2 C repressor to target DNA is detected using anisotropy probed by tryptophan- and tC^O-fluoresence emission. The binding is also detected and measured using Förster resonance energy transfer (FRET) with the FRET-pair tC^O-tC_{nitro} in the target DNA duplex. In an estimation of the binding constant of P2 C repressor to the target DNA helix we found it to be $6 \cdot 10^7$ M^{-1}.

Keywords: DNA, strand exchange, PEG, polyethylene glycol, fluorescent base analogues, P2 C, repressor, binding constant, kinetics

List of Abbreviations

ϵ	Extinction coefficient
Φ_f	Fluorescence quantum yield or quantum yield
τ	Inverted rate constant
k	Rate constant or strand exchange efficiency
A	Adenine
bp	base pair(s)
C	Cytosine
DNA	DeoxyriboNucleic Acid
dsDNA	double-stranded DNA
E.coli	Escherichia coli
FRET	Förster Resonance Energy Transfer
G	Guanine
Na-phos. buffer	Sodium phosphate buffer
operator	DNA binding sequence for a repressor
operon	Initiation sequence of a gene in DNA
PEG	PolyEthylene Glycol (general term)
PEG1000	Polyethylene glycol, $M_W \approx 1000$ g/mol
PEG150	Triethylene glycol, $M_W \approx 150$ g/mol
PEG178	Triethylenglycol-dimethylether, $M_W \approx 178$ g/mol
PEG6000	Polyethylene glycol, $M_W \approx 6000$ g/mol
PNA	Peptide Nucleic Acid
repressor	A protein that is used to control the expression of a gene
RMSE	Root-Mean-Square Error
RNA	RiboNucleic Acid
seleno	selenomethionine-labeled (P2 C repressor)
ssDNA	single-stranded DNA
SSE	Sum of Squared Error
T	Thymine
T_m	Melting temperature of DNA
tC	1,3-diaza-2-oxophenothiazine
tC^O	1,3-diaza-2-oxophenoxazine
tC_{nitro}	7-nitro-1,3-diaza-2-oxophenothiazine
wt	wild-type (P2 C repressor)

Table of contents

1 Introduction

Deoxyribonucleic acid (DNA) is the universal carrier of genetic material for all living cells and exists in the nucleus of eukaryotes and freely moving around in the cytoplasm of prokaryotes (Figure 1.1). Although different, these two types of cells have a lot in common regarding management of the genetic material. [1]

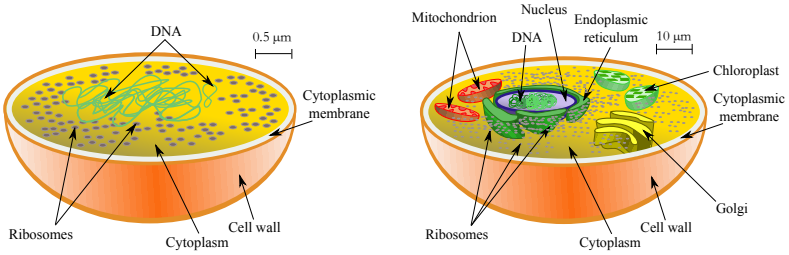

(a) Prokaryotic cell **(b)** Eukaryotic cell

Figure 1.1: Simplified schematic illustration of the internal structure of microbial cells. Note the difference in scale and internal structure, and that eukaryotic animal cells neither contain chloroplasts nor have a cell wall.

One common process is DNA recombination, or exchange of strands between homologous DNA molecules, which occurs in the crowded DNA-rich environment of the cells. This process is vital for all living cells as it plays a key role in both DNA repair and genetic diversity. The *in vivo* reaction is catalyzed by recombination enzymes of for example the RecA family and are very similar in all cell-based organisms [2–5].

In this Thesis the DNA strand exchange is studied using polyethylene glycol (PEG), a synthetic crowding agent with hydrophobic properties, with the purpose to mimic the environment of the active sites of recombination enzymes [6]. To probe this reaction a DNA single strand containing a fluorescent base analogue of the base cytosine, tC^O [7], is used. The specific useful property of this analogue is its high fluoresence when in a single-stranded DNA (ssDNA) and lower in a double-stranded DNA (dsDNA).

Another common process of high importance is the regulation of gene expression. This regulation is governed by proteins that can attach themselves to the dsDNA on positions vital for the expression of the gene in question. By doing so these proteins, from here on called repressors, hinder the ribonucleic acid (RNA) polymerase from transcribing the gene information into RNA.

The second part of this Thesis is to study the binding constant and stochiometry of the P2 C repressor, found in the prokaryote *E.coli* (Escherichia coli), to dsDNA. Also here, tC^O will be used but this time together with its Förster resonance energy transfer (FRET)-acceptor, also a cytosine analogue, tC_{nitro} in the same dsDNA. Using this FRET-pair small changes in dsDNA conformation are detectable through fluorescence variations in tC^O. This is very useful as it is known that the P2 C repressor bends the dsDNA upon binding [8].

2 Theory

This section aims to describe the theory behind the various compounds and methods used in this thesis. This will be combined with the corresponding background information.

2.1 DNA

As a fundamental part of life the DNA serves as the carrier of the genetic information. According to the central dogma of life, as proposed by Crick 1970 [9], DNA serves as a template for the building blocks of life; proteins, as illustrated in Figure 2.1.

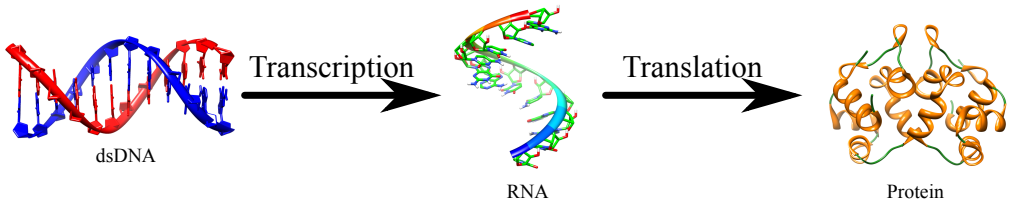

Figure 2.1: Schematic illustration of the central dogma of microbiology. The process from genetic code (DNA) to building blocks of life (proteins).

The DNA duplex, as proposed by Watson and Crick 1953 [10], consists of two polymers. The duplex is often referred to as double-stranded DNA (dsDNA) as opposed to single-stranded DNA (ssDNA) which refers to one of the two polymers required for the duplex (Figure 2.2). The polymers consist of four types of monomeric units, namely the nucleotides adenosine-, thymidine-, guanosine-, and cytidine monophosphate. The monomeric nucleotides consist of a deoxyribose unit, a phosphate unit attached to its 5' carbon position and one of the two purine bases (guanine "G" or adenine "A") or one of the two pyrimidine bases (thymine "T" or cytosine "C") at its 1' carbon position (Figure 2.2a). The dsDNA is held together by hydrogen bonds between the bases and by stacking interactions between bases stacked on top of each orther. Base-stacking, including hydrophobic interactions, is however the main stabilizing factor in the DNA double helix [11, 12].

The most common form of DNA is the B-form where the dsDNA is a right-handed helix and the two single-strands are wound in an anti-parallel fashion about each other. The orientation of the base pairs is almost perpendicular to the helical long axis and there are 10.5 base pairs per helical turn. Each base pair is separated by its stacked neighbor by 3.4 Å. The helical structure of the dsDNA with its major- and minor gooves originates from the way the bases are connected to the DNA backbone. The bases are anchored to the backbone in a way that always puts them closer to the edge of a cross-section circle of the DNA duplex and thus give rise to the major- and minor grooves (Figure 2.3). Two other forms of dsDNA also exist, namely the more compressed right-handed A-form with more turns per length unit than B-form and the left-handed Z-form with fewer turns per length unit than B-form [13] (Figure 2.4).

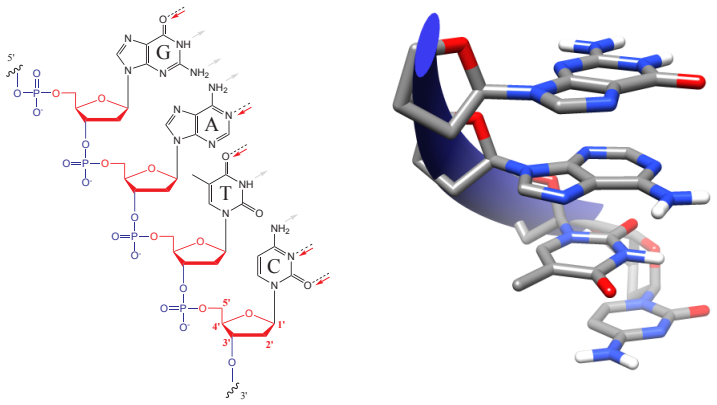

(a) ssDNA oligonucleotide **(b)** ssDNA oligonucleotide in 3D

Figure 2.2: A Lewis-structure of a ssDNA oligonucleotide (a) beginning at the 5'-end with the two purines A & G and ending at the 3'-end with the two pyrimidines T & C. The dashed bonds indicate the potential hydrogen bonds that can be formed, here only marked on the acceptors. The arrow point from the hydrogen bond donor to hydrogen bond acceptor. The different parts of the monomer exemplified at the 3'-end-monomer: deoxyribose unit (**red**), phosphate unit attached to its 5' carbon (**blue**), a base at its 1' carbon (**black**) and a new monomer attaching to its 3' carbon. In the 3D structure (b) the blue ribbon represents the phosphate units (**blue**). Note that the 5' to 3' direction is maintained in both sub figures but the orientation of the individual units is not.

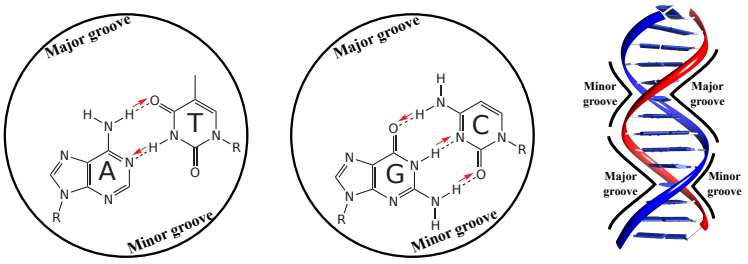

(a) A-T base pairing **(b)** G-T base pairing **(c)** Two kinds of grooves

Figure 2.3: The two natural base pairs (bp) (a) & (b) inside a cross-section circle of the DNA duplex. Dashed bonds indicate hydrogen bonding between the bases, the arrows point from hydrogen bond donor to hydrogen bond acceptor. R = attachment to the backbones of the dsDNA. Illustration (c) indicates the major and minor groove as seen from the side of the B-form DNA duplex.

2.1.1 dsDNA stability

The stability of B-form dsDNA is mainly influenced by four effects. The three constructive effects are hydrogen bonding between the base pairs, the hydrophobic effect and base stacking effects [12], whereas the destructive one is due to the negative charges on the phosphate groups on the DNA backbone (Figure 2.2a).

A major factor in the stability of the duplex is the surrounding environment. It is known that molecules with high hydrogen bonding capabilities, like formamide

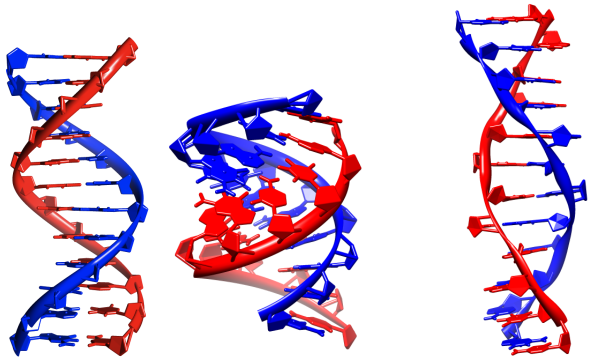

(a) B-form **(b)** A-form **(c)** Z-form

Figure 2.4: The three forms of dsDNA conformations found in biology. All three forms consist of 3 repeats of GATC-base sequence and are thus 12 base pairs long.

and urea, disturb the hydrogen bonds between the base pairs and thereby strongly destabilize the dsDNA [14]. However, during recent years it has been shown that the stacking interactions together with a combination of hydrophobic, dispersive and electrostatic forces are more important for DNA duplex stability and that the CG base-pairing has a stabilizing effect while the AT base-pairing has a slight destabilizing effect on the duplex [12, 15]. In order to investigate the influence of stacking interactions on the DNA duplex a model system, peptide nucleic acid (PNA), was put to use as it lacks the charges residing on the backbone of DNA. In this way the stability of the almost equivalent PNA duplex was studied in organic solutions and indicated that the hydrogen bonding was unaffected but the stacking effects decreased in the presence of the organic solvents dimethylformamide and dioxane. [16, 17]. It is however still difficult to predict the destabilization effect of solvents on the DNA duplex.

Since the DNA backbone is negatively charged (Figure 2.2a) the DNA duplex experiences a repulsive force between the two strands. This can be compensated by the presence of excess cations in the solution surrounding the DNA. The cations will gather in a cloud-like manner around the negative charges to give rise to an over-all charge-neutral environment. This effect is however not purely about Coulomb-forces as there are examples where the nature of the ion is of high importance. Sodium is generally used in order to stabilize the DNA duplex in a solution and also hexahydrated magnesium cations have a stabilizing effect as they bind to DNA (or RNA) to form a supermolecular complex and reduces the negative charge density [18]. Copper (II) however can have high destabilizing effects on DNA [19].

One very useful variable in DNA duplex stability is the temperature. A majority of dsDNAs are stable at room temperature and under physiological conditions strands need not be very long ($\sim$ 40-50 bp) to maintain stability. As temperature rises the DNA duplex becomes more and more unstable and gradually the two strands in the duplex dissociate. The point where the change in concentration of dsDNA occurs fastest is denoted the melting temperature (T_m) of that particular duplex. This temperature is directly used as a measure of the thermal stability of the duplex.

Other than the factors mentioned above, the length of the DNA duplex (to a certain point) influences the value of T_m a lot. It is also possible to derive a theoretically estimated T_m for a duplex of known length and sequence using algorithms available on certain webpages.

2.1.2 DNA strand exchange

DNA strand exchange, the exchange of one single strand in a DNA duplex for another is occurring inside us at all times and is facilitated by recombination enzymes. This system is vital for our survival as damages to our DNA occur frequently and one of the repair-mechanisms is merely to exchange the damaged DNA strand in a duplex for one that is not damaged. Another vital aspect is the exchange of genetic material which is essential for the overall survival of species.

One of the first recombination enzymes to have been characterized is the RecA enzyme of *E.coli.* and its homologs have been found in archaea as well as in eucaryotes [2–5]. The fact that the enzyme underwent minor changes while the vast number of species on our planet evolved to differ quite a lot suggests that the underlying mechanisms involving DNA strand exchange remains highly similar in all forms of life.

The exact action of these recombination enzymes still remains somewhat unclear but during the last few years models have been suggested where the individual enzymes cover the DNA molecule in a helical fashion [20, 21]. The suggested mechanism is that the recombination proteins bind strongly to the DNA single strand in a helical manner as a dsDNA is brought in close proximity to promote the strand exchange (Figure 2.5) [22].

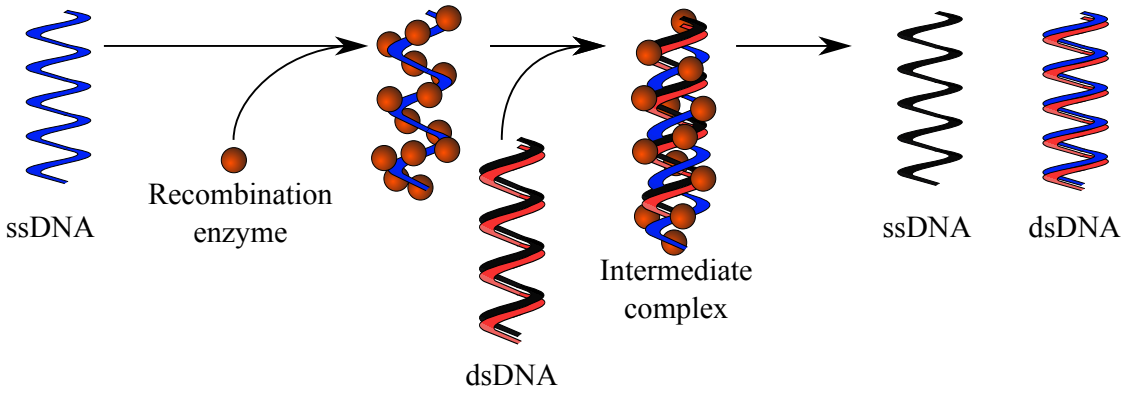

Figure 2.5: Illustration of the suggested mechanism behind the natural DNA strand exchange. The intermediate complex is referred to as a DNA triplex.

2.2 Artificial DNA strand exchange

Artificial DNA strand exchange investigations are today conducted using many different catalyst-acting compounds. At the case where the electrostatic effects are at focus cationic polymers have been widely used. Cationic comb-type polymers consisting of a polylysine backbone are known to increase the strand exchange rate

primarily through their electrostatic interactions with the DNA backbone. In an effort to further investigate the effects of the catalysis due to electrostatic interactions, the experiments were also conducted with polymers containing arginine instead of lysine. Arginine interacts with the DNA through hydrogen bonding as well as electrostatic interactions. This is used as the explanation as to why arginine increases the strand exchange rate more than lysine. [23–25].

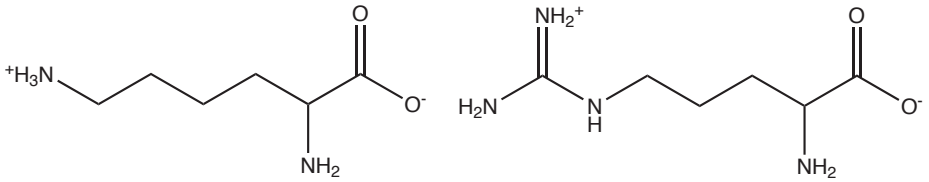

(a) Lysine **(b)** Arginine

Figure 2.6: Lewis structures of Lysine and Arginine.

Another approach is to use positively charged lipids and form liposomes with a surface that attracts DNA and catalyzes the strand exchange. The suggested mechanism states that the liposome surface stabilizes the single strands relative to the duplex. As the DNA opens up in a zipper-like fashion on the surface the probability of strand exchange is increased. A problem encountered using liposomes in this manner is the aggregation upon DNA addition to the mixture. This is prevented by adding small amounts of PEG which minimizes the aggregation but also lowers the DNA strand strand exchange rate[26, 27].

2.2.1 Molecular crowding

Biological macromolecules are developed and function within highly crowded intracellular environments filled by other macromolecules. The results of crowding are seen as large quantitative effects on both the rates and the equilibria of the macromolecules involved. These interactions are commonly studied outside the cell in uncrowded buffers and thus some results are unrepresentative for the real biological environment. This crowded environment can be simulated *in vitro* by adding natural or synthetic macromolecules to the mixtures [28].

This suggests that every species in such crowded environment has an effective concentration which is considerably higher than the normal concentration[29]. Research also suggests that the compact environment *in vivo* helps to stabilize proteins as compared to the common uncrowded environment in a test-tube [30], and also restrains diffusion of different species to a high extent [31, 32].

2.2.2 Polyethylene glycol, PEG

The synthetic non-polar polyethylene glycol (PEG) (Figure 2.7) is a macropolymer that is well suited for simulating the crowding effect found in living cells *in vitro*. An important reason for this is its water solubility which could be assigned to the the special water clustering around the macromolecules [33–35].

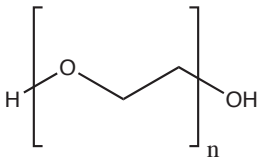

Figure 2.7: Lewis structure of polyethylene glycol (PEG). The factor n generalizes the structure to fit any of the PEG polymers and indicates the number of repeats of the structure within the square brackets.

It has been shown that PEG helps to destabilize the dsDNA and stabilize the strand exchange intermediate state "triplex" (Figure 2.5). The reason for this effect has been assigned to the water-clustering around the duplex [36] and since PEG lowers the water activity [37] the duplex is destabilized. PEG has also been found to enhance DNA polymerase activity as well as protein-protein interactions [38]. These effects are also observed in DNA strand exchange by Feng *et al.* [6].

2.3 Fluorescent base analogues

Ever since its structural discovery in 1953 [10] DNA has been the subject of several structure-, dynamics-, and interaction studies. With the exception of NMR (nuclear magnetic resonance) and crystallography, a normal prerequisite for these studies is accurate and effective labeling or probing techniques.

Fluorescent labeling in the form of fluorescent base analogues to a large extent meet these requirements. The naturally occurring bases in the DNA are virtually non-fluorescent (quantum yield in the order of 10^{-5} [39]) which is why fluorescent base analogues are good probe candidates. There are two characteristic ways to modify a DNA strand by attaching a fluorescent probe molecule. The two ways are external and internal modification and both involve covalent attachment of the fluorophore to an oligonucletide sequence. In the external case the fluorophore is attached outside the actual base stack whereas the internal case corresponds to the fluorophore replacing one of the nucleobases inside the base stack [40].

A good definition of the fluorescent base analogues is given by Wilhelmsson in a review of the field of fluorescent base analogues. The definition states that the analogues should be "significantly fluorescent molecules that resemble the shape of the natural nucleobases and also have some ability to form hydrogen bonds to a base in the complementary strand, i.e., they should not seriously perturb the overall structure of the nucleic acid" [40]. Their usefulness is therefore directly proportional to how well they meet the criteria stated in the definition.

One of the first fluorescent base analogues, discovered by Ward *et al.* in 1969, was the highly fluorescent adenine analogue 2-AP (2-aminopurine) [41]. This analogue has been used as a probe in several different fields due to its ability to form base pairs with thymine and uracil and also being one of the few commercially available fluorescent analogues. One of the fields utilizing the analogue involves genetic regulatory elements, riboswitches, found commonly in bacterial mRNA [42, 43]. Other adenine analogues, like 6-MAP and DMAP in the pteridine-group, have been developed along with guanine analogues 3-MI and 6-MI by Hawkins *et al.* [44, 45]. These analogues also show great promise but 3-MI, and to some extent also 6-MAP and DMAP, render the DNA double helix less stable [45].

The parent of the analogues used in this thesis is the tricyclic cytosine analogue 1,3-diaza-2-oxophenothiazine (tC) (Figure 2.8a), originally developed in 1995 [46], which was found to be highly fluorescent and have just about the same quantum yield in monomeric, PNA single-strand and PNA-DNA hybrid duplex form [47].

The oxo-homolog 1,3-diaza-2-oxophenoxazine (tC^O, used in this Thesis, Figure 2.8b) was developed at the same time as tC but the photophysical characterization was reported later (2008) showing a high quantum yield in duplex form with a mono-exponential decay [7]. It is considered on average in different duplex contexts the brightest fluorescent base analogue available today [40].

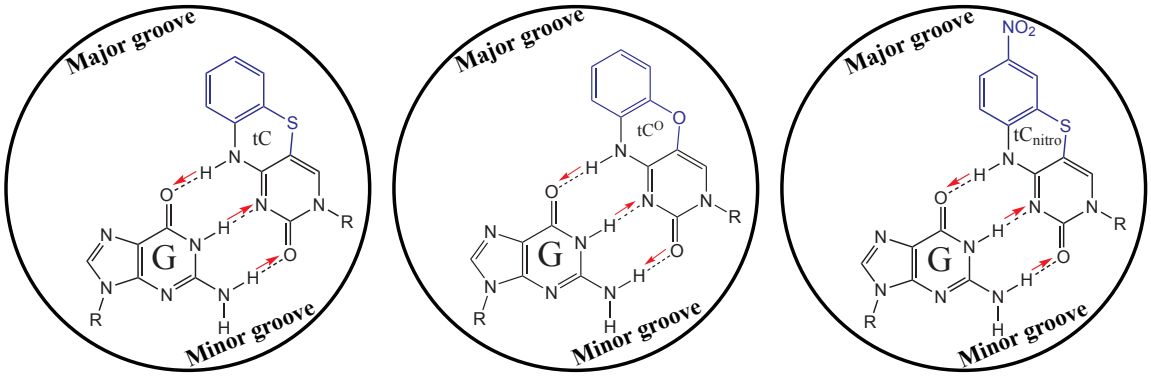

(a) tC **(b)** tC^O **(c)** tC_{nitro}

Figure 2.8: Lewis structures of the cytosine analogues in the tC-family base paired with guanine inside a cross-section circle of the DNA duplex. Dashed line indicates hydrogen bonding between the bases and the arrows point from hydrogen bond donor to acceptor. The blue part of the analogues structure highlights the part that deviates from the natural cytosine structure. R = attachment to the DNA backbone.

The properties of both tC and tC^O make them well suited as FRET donors [40]. However, until 2009 there was a lack of useful FRET-acceptor base analogues with descent properties. In an effort to fill this gap Wilhelmsson *et al.* developed the FRET-acceptor 7-nitro-1,3-diaza-2-oxophenothiazine, tC_{nitro}, (also used in this Thesis, Figure 2.8c) thus forming a new FRET pair consisting of tC^O as the donor and tC_{nitro} as the acceptor [48]. With the new acceptor a high orientational control of the FRET pair was enabled and at the same time there was merely a minimal perturbation to the structure and stability of the nucleic acid [49].

2.3.1 The FRET-pair tC^O & tC_{nitro}

The base analogues tC^O and tC_{nitro} (used in this Thesis) constitute the first nucleobase analog FRET-pair. This FRET-pair has successfully been used to monitor the nucleobase distances and orientations covering more than one turn of the DNA duplex. The excellent control of the donor and acceptor geometry and position could be monitored as a very distinct FRET change as the distance between tC^O & tC_{nitro} increased and orientation changed. It is now possible to use these base analogues in various studies regarding conformational changes of the DNA duplex. [48]

The donor of the FRET-pair, tC^O(Figure 2.8b), is highly fluorescent both as free nucleoside and incorporated into a DNA structure. In its free nucleoside form, the lowest energy absorption band is found at 360 nm ($\epsilon_{360\ nm} = 9000\ M^{-1}cm^{-1}$) with its fluorescence peak at 465 nm and a quantum yield, Φ_f, of 0.3. The lowest absorption band is slightly ($3 - 10$ nm) red-shifted as tC^O is embedded in either single or double stranded DNA and the quantum yield (Φ_f) is found to be approximately 0.22. Furthermore it was found that tC^O base paired exclusively with guanine with only a minor tendency for base-flipping and overall provided merely minimal perturbation to the native DNA structure. [7].

It was also found that the tC^O increases the stability of the DNA duplex with regard to the melting temperature by on average 2.7 °C. Along with this discovery it was observed that if a purine resides on the 5'-side of the analogue in dsDNA, the effect on the melting temperature (T_m) is on average 0 °C, while having a pyrimidine on the 5'-side increases T_m on average by 5 °C [7]. As a consequence of this, it is possible to choose a tC^O-labeled DNA sequence in such a way that the effect of tC^O on the DNA helix stability is further minimized.

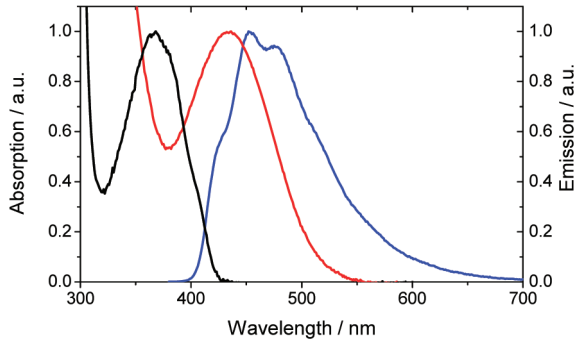

Figure 2.9: Normalized absorption (**black**) and emission (**blue**) spectra of the FRET donor $tC^O$and absorption spectrum (**red**) of the virtually non-fluorescent acceptor tC_{nitro} in dsDNA. Note the spectral overlap of tC^O emission (**blue**) and tC_{nitro} absorption (**red**). [This graph is taken from the tC^O-tC_{nitro}-FRET article of Börjesson *et al.* The measurements were performed at 22 °C in 25 mM phosphate buffer (pH 7.5) and [Na^+] 100 mM [48]]

The acceptor of the FRET-pair, tC_{nitro} (Figure 2.8c), is non-fluorescent with the lowest absorption band centered at 424 nm ($\epsilon_{424\ nm} = 5400\ M^{-1}cm^{-1}$) which gives a good overlap with the tC^O-emission centered at 465 nm (Figure 2.9) [48, 49].

Like the donor, tC_{nitro} gives minimal perturbation to the stability and structure of dsDNA even though tC_{nitro} is not fully planar. The slightly folded structure along the middle sulfur-nitrogen axis however has only minute effects on the DNA duplex structure as the size-expanded tC_{nitro} (and tC^{O}) extends into the major groove of the DNA duplex (Figure 2.8b & c). Given the structural similarities of tC^{O} and tC_{nitro} it is also considered likely that they have similar and low base-flipping rate. [49]

2.4 Proteins

Proteins are the building blocks of life and are the result of the expressed genetic information, in accordance with the central dogma as proposed by Crick [9] (Figure 2.1). They consist of one or more peptides and each peptide consists of several amino acids, or in other words a polymer of amino acids.

Proteins play a variety of roles, some in the cells and others outside. Some of their purposes may be to transport or to store small molecules, to make up the structural framework of cells and tissues, mediate muscle contraction, being part of the immune system or blood clotting and also to regulate gene expression. Some of the most important proteins are the enzymes that catalyze and regulate the enormous veriety of reactions that are essential for life. Every type of cell has several thousand types of proteins that are serving their individual purposes at any given time. [50]

An important type of protein is repressors that can bind to a part (an operator) of the initiation sequence of a gene (an operon) and thus physically block the binding of RNA polymerase, preventing it from transcribing the gene sequence to RNA. The repressor generally also has a binding site for an inducer which controls the activity of the repressor. An inducer, when bound to a repressor, greatly reduces the repressors affinity for DNA. [50]

2.4.1 The P2 C repressor

The P2 C protein, which exists in *E.coli*, is an immunity repressor of the temperate *E.coli* phage P2 virus. Once an *E.coli* is infected with the virus the viral reproduction starts in one of two ways; the lytic cycle or the lysogenic cycle. The most common and effective virus-spreading approach is to force the infected cell into the lytic cycle. Here the viral DNA utilizes the machinery of the cell to produce more encapsulated viruses and when a critical amount is reached the host cell is destroyed so that the new viruses can spread to other cells. The other approach is for the virus to simply incorporate its DNA into the hosts genome (plasmid) and reproduce its own genome along with the host's during cell division, thus not destroying the cell. [1] The later is called the lysogenic cycle and the requirement for the temperate *E.coli* phage P2-infected *E.coli* to enter this cycle is the presence of the P2 C repressor [8].

Contradictory to most prokaryotic repressors, the P2 C repressor binds to non-palindromic direct repeats of DNA sequences and it shares this property with most repressors of the P2-like *E.coli* viruses. The determined structure of the P2 C re-

pressor indicates that it consists of two symmetric monomers oriented in a way to enable the dimer to bind in to the major groove of two subsequent turns of the DNA helix (Figure 2.13). The lower helices of the repressor are found to be responsible for the recognition of the binding site on the DNA duplex through alanine scanning, thus implying the importance of the individual protein residues concerning DNA recognition. Since the gene of interest here has two operator-sites in its operon, a successful repression requires two P2 C repressors to bind to the DNA, one at each site. [8] As indicated in Figure 2.10b it is hypothesized that this binding results in bending of the DNA duplex [8] since many repressors of the P2 C repressor-family display this property [51].

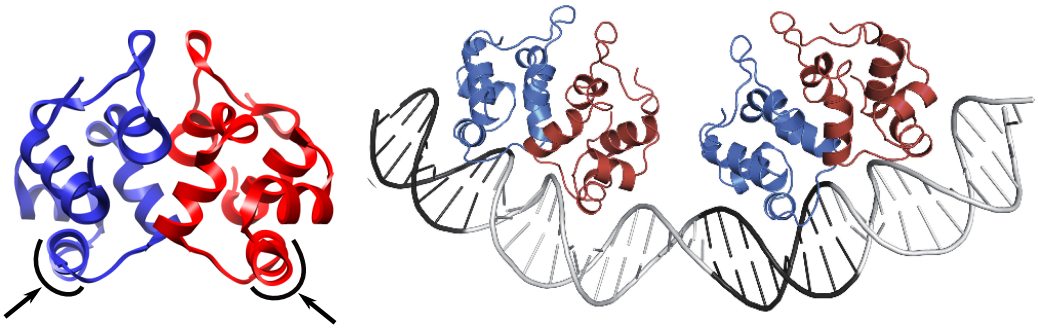

(a) P2 C repressor **(b)** Two P2 C repressors binding to DNA

Figure 2.10: (a) A 3D illustration of the P2 C repressor consisting of two symmetric monomers, here represented in blue and red. The two lowest helices (one of each monomer, indicated by black lines and arrows) interact with the DNA duplex. (b) A hypothetical mode of the binding between two P2 C repressors and a DNA duplex. Note the bending of the dsDNA. [The model illustration is taken from Crystal structure of the P2 C-repressor-article by Massad *et al.* [8]]

2.5 Absorption spectroscopy

Absorption of electromagnetic radiation in the UV-vis region involves exciting molecules from their ground state to a higher excited state. It is the molecule that absorbs the energy of the light, provided that the energy fits the energy gap between two molecular electronic states. If this condition ($\Delta E = h\ \nu$) is not met the excitation cannot occur.

Absorption (A) of a sample at the wavelength λ can be calculated using the Beer-Labert law

$$A = -log\left(\frac{I}{I_0}\right) = \epsilon\ l\ c \tag{2.1}$$

where I is the light intensity after passing through the sample, I_0 is the intensity of the light before passing through the sample, ϵ [$cm^{-1}M^{-1}$] is the specific extinction coefficient of the molecule , l [cm] is the length of the path the light travels through the sample and c [M] is the concentration of the sample.

2.5.1 Spectrophotometer

The instrument used to perform absorption spectroscopy is called a spectrophotometer. A light source is used to produce light containing a wide range of wavelengths. The light from the light source is divided using a monochromator and by rotating the monochromator the wanted wavelength can be directed through the sample. When the light passes the sample it is recorded using a detector. See fig. 2.11 for a schematic illustration.

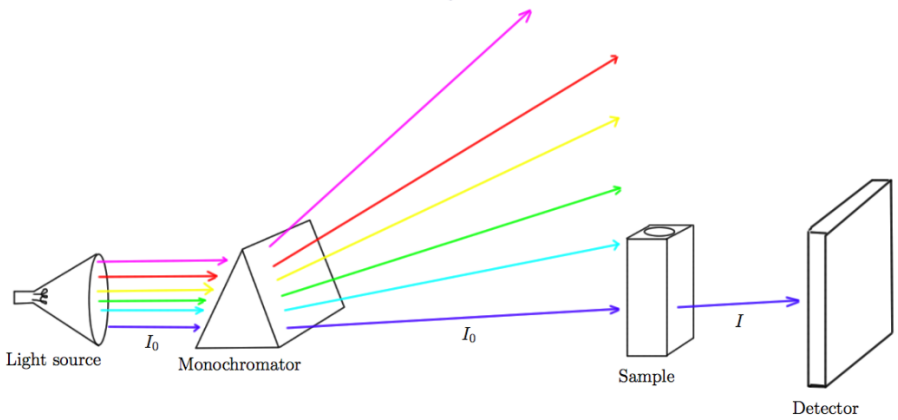

Figure 2.11: A schematic illustration of an absorption spectrophotometer.

2.6 Fluorescence spectroscopy

When a molecule absorbs light of a certain wavelength it must eventually get rid of that energy. A simplified Jablonski diagram (fig. 2.12) represents the different types of energy states that a molecule can be excited to and the different ways it can return to the ground state. The non-radiative paths are: internal conversion, vibrational relaxation, intersystem crossing.

If a molecule returns to the ground state from the first singlet state via a radiative path, light is emitted. This light is called fluorescence and has longer wavelength and hence lower energy than the absorbed light. If the radiative relaxation occurs via the triplet state, the emission is perceived as phosphorescence. However this requires a non-radiative intersystem crossing to occur first. Alternatively the molecule can return to the ground state from the first singlet state via internal conversion and vibrational relaxation in which case no light is emitted (Figure 2.12).

A way to calculate the fraction of energy-relaxation that occurs via a specific path is called quantum yield. For the fluorescence quantum yield the following expression can be used

$$\Phi_f = \frac{k_f}{k_f + k_{ic} + k_{isc}} \tag{2.2}$$

where Φ_f is quantum yield of fluorescence and k_f, k_{ic} and k_{isc} are the rate constants

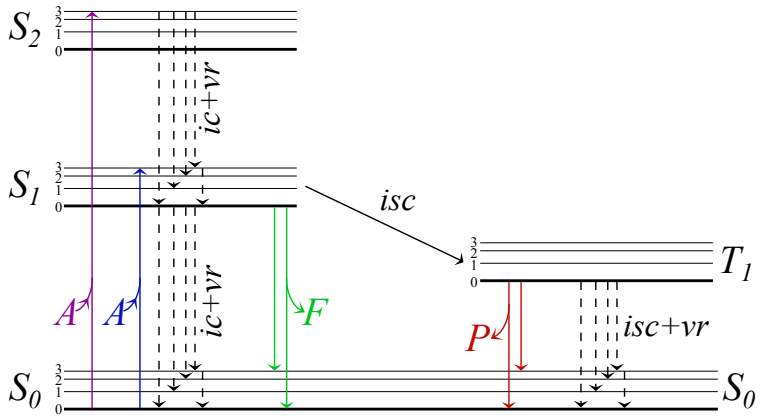

Figure 2.12: A simplified illustration of the Jablonski diagram. The abbreviations are A: Absorption, $ic + vr$: internal conversion and vibrational relaxation, F: fluorescence, isc: intersystem crossing, P: phosphorescence, S: singlet states, T: triplet states. The thick and thin black lines represent the lowest and higher vibrational levels of each state respectively.

for fluorescence, internal conversion and intersystem crossing, respectively. These rate constants are only considered from the first singlet state (S_1) to the ground state (S_0) since it is between these states that the rates are slow enough to give a significant contribution to the calculations. A simplified expression would be

$$\Phi_f = \frac{\text{Photons out}}{\text{Photons in}} = \frac{\text{Fluorescence rate}}{\text{Fluorescence rate} + \text{Non-radiative rates}}$$

2.6.1 Spectrofluorimeter

Emission spectroscopy is performed in a spectrofluorimeter. The spectrofluorimeter excites the sample in the same manner as the spectrophotometer does (Figure 2.11) and then detects the emission of light from the sample. It normally contains two monochromators, one to control the excitation wavelengths and one to filter the emission wavelengths right before the detector.

There are mainly two different ways to utilize a spectrofluorimeter. One can measure the excitation of the sample by recording one emission wavelength while varying the excitation wavelength or the other way around, to measure emission while the excitation wavelength is kept constant.

2.7 DNA binding constant of the P2 C repressor

When deriving the equation for the binding constant of the P2 C repressor it was initially assumed that no cooperativity occurred upon binding. This simplification means that both P2 C repressors binds to the two binding sites on the DNA duplex at the same time without any interactions between each ohter (Figure 2.13a). The other more complex case is when one of the two binding moieties bind first and changes the binding affinity of the second moiety (Figure 2.13b).

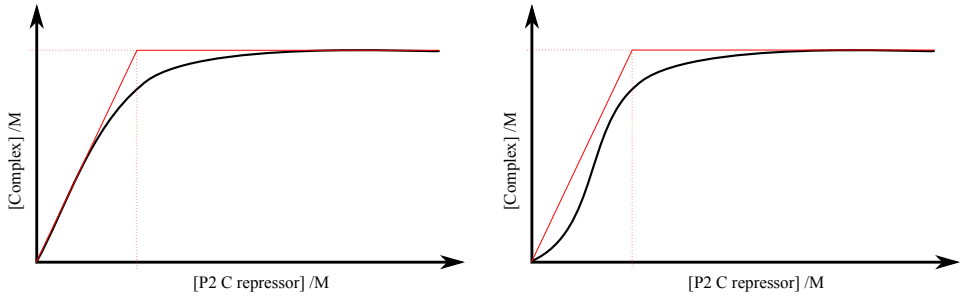

(a) Non-cooperative binding **(b)** Cooperative binding

Figure 2.13: Schematic illustrations (P2 C repressor + dsDNA complex concentration Vs. P2 C repressor concentration) of two types of binding curves, one non-cooperative (a) and one with cooperativity (b). The diagonal and horizontal red lines indicate the way the binding curve would go if the binding constant K was infinitely large. As K is lowered the transition of the binding curve from the binding area (roughly to the left of the vertical doted red line) to the full-bound area (roughly to the right of the vertical dotted red line) occurs more smoothly.

Following this first approximation of non-cooperative binding of the two P2 C repressors to dsDNA, the following reaction without any intermediate steps is assumed to take place.

$$\mathrm{dsDNA_{free}} + (\text{P2 C repress})_{2\ free} \rightleftharpoons \mathit{Complex} \tag{R 2.1}$$

The binding constant for reaction R 2.1 would then be

$$K = \frac{[\mathit{Complex}]}{[\mathrm{dsDNA}]_{free}\,[(\text{P2 C repress})_2]_{free}} \tag{2.3}$$

where the square brackets indicate the concentration of the moiety inside them. The relation for the concentration of the *Complex* is given by

$$\begin{aligned} [(\text{P2 C repress})_2]_{tot} &= [(\text{P2 C repress})_2]_{free} + [\mathit{Complex}] \Rightarrow \\ x &= [(\text{P2 C repress})_2]_{free} + y \end{aligned} \tag{2.4}$$

and for the dsDNA we have that

$$\begin{aligned} [\text{dsDNA}]_{tot} &= [\text{dsDNA}]_{free} + [Complex] \Rightarrow \\ c &= [\text{dsDNA}]_{free} + y \end{aligned} \tag{2.5}$$

Mind the replacement of variables. By combining equations (2.3), (2.4) and (2.5) we get the expression

$$K = \frac{y}{(c-y)(x-y)} \tag{2.6}$$

which can be rearranged[1] into

$$y = \frac{1 + c\ K + K\ x - \sqrt{c^2K^2 - 2\ c\ K^2x + 2\ c\ K + K^2x^2 + 2\ K\ x + 1}}{2\ K} \tag{2.7}$$

where c [M] is the constant concentration of dsDNA in the mixture, x [M] is the increasing concentration of P2 C repressor protein as a result of the stepwise addition, and y [M] is the measured concentration of the formed *Complex*.

The expression in equation (2.7) is fitted to the raw data of the P2 C repressor-dsDNA binding titration to get the binding constant, K.

2.8 Kinetic modeling of strand exchange

The model used for extrapolating the rate constant of DNA strand exchange is that of single exponential decay, given as

$$F(t) = F^*_\infty - \Delta F\ e^{\left(\frac{-t}{\tau}\right)} \tag{2.8}$$

where $F(t)$ [a.u.] is the fluorescence emission at any given time t [s], ΔF [a.u.] is the difference between emission at the beginning of the measurement and F^*_∞ [a.u], and F^*_∞ [a.u.] which is the emission at the end of the kinetics measurement (preferably when the reaction has reached its equilibrium). τ [s] is the inverted rate constant, and consequently

$$k = \frac{1}{\tau} \tag{2.9}$$

1. The rearrangement is done in MATLAB R2010B

where k [s^{-1}] is the rate constant or the efficiency of the reaction [6].

The expression for calculating reaction yield is

$$Y(t) = \frac{F(t) - F_0}{F_\infty - F_0} \tag{2.10}$$

where the $Y(t)$ and $F(t)$ are the reaction yield and fluorescence emission respectively at any given time t. F_0 is the fluorescence emission of the reference sample that has not undergone strand exchange and F_∞ is the fluorescence emission of a sample that is synthetically equilibrated through re-annealing.

In an ideal case where the measurement and the reaction are started simultaneously and equilibrium is reached in a reasonable amount of time, we would have that

$$F_\infty = F_\infty^* \tag{2.11}$$

and subsequently that

$$F_0 = F_\infty - \Delta F \tag{2.12}$$

This can however be hard to achieve.

2.9 Förster resonance energy transfer, FRET

The FRET-technique is used in this Thesis to monitor the binding of the P2 C repressor to a DNA duplex labeled with the tC^O-tC_{nitro} FRET-pair. The excited donor (in this case tC^O) can transfer its excited-state energy to the acceptor (tC_{nitro}) by non-radiative interaction due to their transition dipole moments. Although the transfer process between the chromophores is non-radiative, the absorption of the acceptor needs to overlap with the emission spectrum of the donor.

FRET is very distance sensitive, as indicated by the sixth powers on the distances in equation (2.13)

$$E = \frac{R_0^6}{R_0^6 + r^6} \tag{2.13}$$

where E is the energy transfer efficiency, R_0 is the distance where the probability of energy transfer is 50% and is called the Förster distance [52], and r is the distance between the chromophores. It is this distance sensitivity that makes FRET useful in studies where small distances or small changes in distances are to be monitored.

2.10 Anisotropy

Anisotropy is used in this thesis to probe the P2 C repressor binding to dsDNA by detecting the slower rotation of the P2 C-dsDNA complex relative to either the dsDNA or the P2 C repressor itself.

A necessity for anisotropy is the existence of a majority of transition dipole moments directed along a specific direction in the sample. In a homogenous solution the fluorophores and their transition dipole moments are oriented randomly. Upon exposure to polarized light mainly those fluorophores that have their absorption transition moments aligned with the electronic vector of the incoming light will be excited. After the moment of excitation all fluorophores continue to rotate and move around randomly. If the fluorescence emission occurs faster than the angular displacement of the fluorophores anisotropy can be detected. If however the angular displacement is much faster than the fluorescence lifetime, a majority of the photons emitted will have differently oriented polarizations and thus minimal or no anisotropy will be detected.

Anisotropy is therefore a measurement of the average angular displacement of a fluorophore relative to its fluoresence lifetime. Anisotropy is largely independent of the concentration of the fluorophore itself[2] but is dependent on the size and shape of the fluorophore as well as the viscosity of the solvent used.

The following formula is used in this Thesis for calculating anisotropy

$$r = \frac{I_{VV} - G\ I_{VH}}{I_{VV} + 2\ G\ I_{VH}} \tag{2.14}$$

and G is a compensation factor for polarization due to the monochromator in the spectrofluorimeter and is defined as follows

$$G = \frac{I_{HV}}{I_{HH}} \tag{2.15}$$

where I stands for the detected emission and its subscripts V and H for vertical- and horizontal polarization, respectively. The first subscript of I indicates how the incoming light is polarized and the second subscript how the emitted light is polarized, *i.e.* how the polarizers are positioned. r is the detected anisotropy. [53]

2. Extreme concentrations may have an effect on anisotropy in both directions.

3 Materials and Methods

This section contains specific information about all the compounds used in this Thesis as well as the instruments used. It also contains a brief description of the experimental procedures regarding each of the two projects.

3.1 Instrumentation

3.1.1 Spectrophotometer

Absorption spectra were recorded using a Varian Cary 4000 or a Varian Cary 5000 UV-vis Spectrophotometer (Varian, USA). Scans were recorded between 200 nm and 500 nm with the average time of 0.1 s, fixed SBW at 1 nm, beam mode set to double and slit height reduced. A 1.5 mL reduced quartz fluorescence cuvette was used.

Melting temperatures of the different DNA duplexes were recorded on the same Varian Cary 4000 UV-vis Spectrophotometer (Varian, USA) equipped with multicell thermal block at 260 nm. SBW was set to 1 nm, average time 3 s and internal temperature probe in MiliQ-H_2O was used as temperature reference. Number of thermal stages was set to 4 with the starting temperature at 15 °C and ending temperature at 25 °C. Data interval was set to 0.5 °C and rate was set to 0.5 °C/min. The 4 stages were set according to

$$\begin{aligned}(15\ ^\circ\text{C}) \xrightarrow{Stage\ 1} 95\ ^\circ\text{C},\ [\text{hold 5 min}] \xrightarrow{Stage\ 2} 5\ ^\circ\text{C} \\ \xrightarrow{Stage\ 3} 95\ ^\circ\text{C},\ [\text{hold 5 min}] \xrightarrow{Stage\ 4} 5\ ^\circ\text{C} \xrightarrow{Return} (25\ ^\circ\text{C})\end{aligned}$$

and were run over night. Four quartz absorbance cuvettes were used for the recording of the melting temperatures.

3.1.2 Spectrofluorimeter

Two different spectrofluorimeters were used in the two different projects, mainly due to sensitivity reasons.

DNA strand exchange project

Fluorescence emission spectra for the DNA strand exchange project were recorded using a multicell thermoregulator equipped Varian Cary Eclipse fluorometer (Varian, USA) in 1.5 mL reduced quartz fluorescence cuvettes. Excitation wavelength was set at 375 nm with excitation slit at 10 nm and emission scan was set between $385 - 700$ nm with emission slit at 5 nm and scan control was set to medium.

Fluorescence kinetics traces for the DNA strand exchange were performed using the same instrument in 1.5 mL reduced quarts fluorescence cuvette. Excitation wavelength was set to 375 nm with excitation slit at 10 nm and emission wavelength set to 455 nm with emission slit at 5 nm. Simple collection was chosen with average time of 1 s and 1 stage with cycle time of 0.25 min and a stop time at 300 min. PMT Detector voltage was set to medium (600 V), the multicell holder temperature

control was set to 39 °C resulting in 37 °C in the cuvettes. The temperature of the block was monitored.

P2 C repressor project

The fluorescence emission scans for the P2 C repressor project were preformed on Spex Fluorolog 3 spectrofluorimeter (JY Horiba). The excitation wavelength was set to 375 nm with excitation slits at 3 nm and emission was detected between 385 - 700 nm with emission slit at 3 nm. Integration time was set to 0.2 s.

Anisotropy measurements using tC^O as the probe and the same instrument as above were preformed with excitation ranging between 330 - 440 nm with excitation slit at 5 nm and emission detection set at 455 nm with emission slit set to 5 nm. Integration time was set to 0.5 s.

Anisotropy measurements using the P2 C intrinsic tryptophan as the probe and the same instrument as above were preformed with excitation wavelength ranging between 270 - 340 nm with excitation slits at 5 nm and emission was recorded at 350 nm with emission slits at 5 nm. Integration time was set to 0.5 s.

3.2 DNA

The DNA sequences used in this project were purchased from ATDBio Ltd, Southampton. The strands are delivered freeze-dried and upon arrival diluted in 1 mL MilliQ-H_2O for the DNA strand exchange study and in 0.5 mL MilliQ-H_2O for the P2 C repressor study, to ensure adequate stock concentrations. After dilution the stock was divided in to 100 μL volumes in 500 μL screw-cap tubes as a precautionary measure to ensure minimal risk for contamination in the stock.

The strands used in the DNA strand exchange project are found in Table 3.1 and those used in the P2C repressor project are found in Table 3.2.

Table 3.1: DNA strands for DNA strand exchange project. The production names of the strands are replaced by more convenient strand labels for easier reference. (For full names see Table 10.1 in Appendix 10.1) The position of the used base analogue, tC^O, is indicated by **X** in the 38 monomer long DNA sequences and their respective ϵ is found in the rightmost column. Note that the sequences are given in 5' to 3' direction while the complementary strand is given in 3' to 5' direction.

Strand label	DNA sequences (38-mer)	ϵ_{260nm} [M^{-1} cm^{-1}]
S_1	5'-CCT **X**AC ACA CAT GCA GAG AGA GAG TGC ACA CAC ACA CC-3'	388 710
S_2	5'-CCT CA**X** ACA CAT GCA GAG AGA GAG TGC ACA CAC ACA CC-3'	388 710
S_3	5'-CCT CAC A**X**A CAT GCA GAG AGA GAG TGC ACA CAC ACA CC-3'	388 710
S_4	5'-CCT CAC ACA **X**AT GCA GAG AGA GAG TGC ACA CAC ACA CC-3'	388 710
S_5	5'-CCT CAC ACA CAT GCA GAG AGA GAG TGC A**X**A CAC ACA CC-3'	388 710
S_6	5'-CCT CAC ACA CAT GCA GAG AGA GAG TGC ACA **X**AC ACA CC-3'	388 710
S_7	5'-CCT CAC ACA CAT GCA GAG AGA GAG TGC ACA CA**X** ACA CC-3'	388 710
S_8	5'-CCT CAC ACA CAT GCA GAG AGA GAG TGC ACA CAC A**X**A CC-3'	388 710
S_{unmod}	5'-CCT CAC ACA CAT GCA GAG AGA GAG TGC ACA CAC ACA CC-3'	385 470
S_{compl}	3'-GGA GTG TGT GTA CGT CTC TCT CTC ACG TGT GTG TGT GG-5'	353 790

Table 3.2: DNA strands used in the P2 C repressor project. The production names of the strands are replaced by more convenient strand labels for easier reference. (For full names see Table 10.7 in Appendix 10.2) The positions of the used base analogues tC^O and tC_{nitro} are indicated by **X** and **Y**, respectively, in the 54 monomers long DNA sequences. The calculated extinction coefficients at 260 nm are found in the rightmost column. Note that the sequences are given in 5' to 3' direction while the complementary strand is given in 3' to 5' direction.

Strand label	DNA sequences (54-mer)	ϵ_{260nm} $[M^{-1}cm^{-1}]$
P_1	5'-GTT TGA CAT GGT GTT TAG AT**X** TCA ATA GTA TTT CGT TTA GAT GTA GAT TGT TTA-3'	545 580
P_2	5'-GTT TGA CAT GGT GTT TAC ATC TCA ATA GTA TTT **X**GT TTA GAT GTA GAT TGT TTA-3'	545 580
P^*_{comp}	3'-CAA ACT GTA CCA CAA ATC TAG TGA TAT **Y**AT AAA GCA AAT CTA CAT CTA ACA AAT-5'	578 430
P_{unmod}	5'-GTT TGA CAT GGT GTT TAC ATC TCA ATA GTA TTT CGT TTA GAT GTA GAT TGT TTA-3'	542 340
P_{comp}	3'-CAA ACT GTA CCA CAA ATC TAG TGA TAT CAT AAA GCA AAT CTA CAT CTA ACA AAT-5'	575 460

3.2.1 Calculation of extinction coefficients

The extinctions coefficients (ϵ) for ssDNA at 260 nm were calculated using a linear combination of the extinction coefficients of the individual bases at 260 nm. To account for the base-stacking effect the linear combination was multiplied by 0.9 to make the final estimate as accurate as possible, according to the expression below

$$\epsilon_{ssDNA,260nm} = 0.9 \left(\sum_i N_i \ \epsilon_{i,260nm} \right) \tag{3.1}$$

where $i = \{A, T, C, G, tC^O, tC_{nitro}\}$, N is the number of bases i in the ssDNA and $\epsilon_{i,260nm}$ is the extinction coefficient of the base i in the single strand [7, 54] (Table 3.3).

Table 3.3: The extinction coefficient for the individual natuaral bases as well as the fluorescent analogues tC^O and tC_{nitro}.

Bases	ϵ_{260nm} $[M^{-1}cm^{-1}]$
Adenine	15 300
Tyrosine	9 300
Cytosine	7 400
Guanine	11 800
tC^O	11 000
tC_{nitro}	10 700

3.2.2 DNA annealing

DNA duplexes were made from the ssDNA by mixing the proper amount of each single strand, increasing the temperature to 95 °C and linearly lowering it to 5 °C during 12 hours. This allows the majority of already formed duplex structures to dissociate fully (since T_m is much lower than 95 °C for natural DNA duplexes) and slowly associate again, preferably so slow that the temperature descent becomes the limiting factor in the duplex-forming reaction. The annealing process is preformed

in a temperature controlled water bath usually over night. The complementary strands of the tC^O-labeled ssDNA were always added in excess to ensure that all tC^O strands end up in DNA duplex form.

3.3 The DNA strand exchange project

The first step of this project was to make the buffer needed for the strand exchange. Then the suitable DNA strands were chosen from the available ones (Table 3.1) by comparing their T_m with an unmodified duplex of the same sequence. This was followed by careful project planning and sample preparation. Once the sample stock was prepared with the reference- and trace samples, kinetics experiments were performed in buffer and in different forms of PEG at 37 °C.

3.3.1 Buffer

A stock of 500 mL sodium phosphate buffer (Na-phos. buffer) containing 50 mM Na^+ and 1 mM EDTA was prepared by adding 0.298 g NaH_2PO_4, 2.041 g $NaHPO_4$, 1 mL EDTA and diluting up to less than 500 mL with MilliQ-H_2O. The pH was adjusted to 7.51 using diluted HCl/NaOH followed by an addition of MilliQ-H_2O to a final volume of 500 mL. The buffer was then filtered through micropore filter (pore diameter 0.45 μm) and stored in two 250 mL bottles at 4 °C.

3.3.2 PEG

All PEG-solutions were prepared at 50% by weight concentration of PEG-sodium phosphate buffer. After adding the buffer to equal weight of PEG in a 50 mL TPP® tube, the two species were mixed by slow rotation for 30 minutes until a homogenous solution was obtained. The mixture was allowed to rest for a minimum of three days before usage and always kept at room temperature ($\sim$ 22 °C). The different PEGs used in this project are presented in Table 3.4 and their Lewis structures are seen in Figure 3.1. All four chemicals were bought from Sigma-Aldrich with a purity of $\geq$ 99%.

Table 3.4: The different variations of polyehtylene glycoles used in this Thesis.

Chemical name	Chemical formula	Molecular weight [g/mol]	Abbreviation used
Polyethylene glycol	$(C_2H_4O)_nH_2O$	~6000	PEG6000
Polyethylene glycol	$(C_2H_4O)_nH_2O$	~1000	PEG1000
Triethylene glycol	$(C_2H_4O)_3H_2O$	150.171	PEG150
Triethylenglycol-dimethylether	$CH_3O(C_2H_4O)_3CH_3$	178.23	PEG178

3.3.3 Choice of candidate strands

It was desirable to perform DNA strand exchange experiments using labeled DNA duplexes that were as equal as possible to the correspoinding unmodified DNA duplex in terms of stability and structure. To find such duplexes, melting temperatures of all possible duplexes from the strands in Table 3.1 needed to be examined. Each

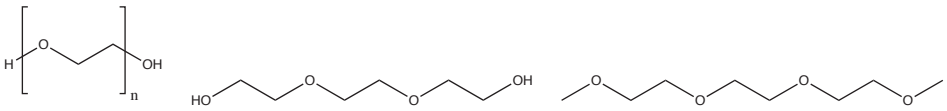

(a) PEG1000/ PEG6000 **(b)** PEG150 **(c)** PEG178

Figure 3.1: The Lewis structures of the three different PEGs used in this Thesis.

of the single strands (S_1-S_8 and S_{unmod}) were diluted to a total volume of 2 mL and 2.5 μM while the complementary strand S_{compl} was made up to 6 mL and 3 μM. A volume of 650 μL of each single strand was mixed with 650 μL S_{compl} with 2% higher concentration to ensure that all the labeled ssDNA form duplexes. Stage 1 and 2 served as the annealing process to form duplexes in the melting temperature experiment (Section 3.1.1).

For comparison the average temperatures, obtained through the steepest gradient of the melting curves as well as the half-temperature method (Figure 3.2), from stage 3 and 4 in the melting temperature experiment (Section 3.1.1), were used and compared with that of the unmodified duplex. This suggested which duplexes were most suitable to use with regard to thermal stability.

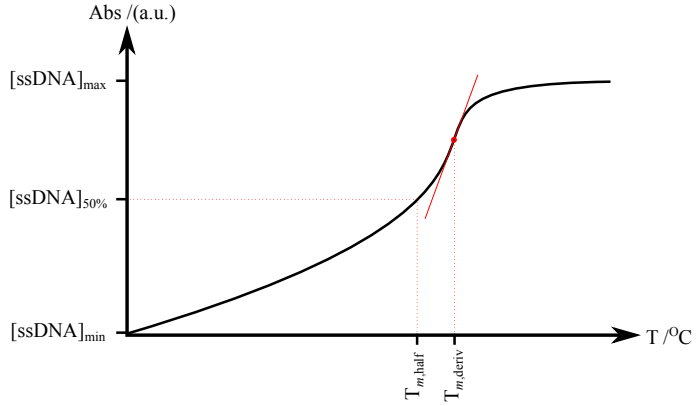

Figure 3.2: The two ways of reading melting temperatures of a melting curve for dsDNA. The $T_{m,\text{half}}$-temperature depends on where half of the maximum ssDNA concentration is and $T_{m,\text{deriv}}$ depends on where the dissociation reaction occurs the fastest as a function of temperature, here indicated by the sloping red line and a dot to mark the spot.

Another important property that was desired in the chosen strands was a large difference in fluorescence emission between single and double stranded forms, or so called "good contrast". This was investigated using a spectrofluorimeter (Section 3.1.2) on the single strands (S_1-S_8, Table 3.1) and on the duplexes after the melting temperature experiments.

3.3.4 Kinetic traces

The design of the experiment was to start with a DNA duplex containing one of the chosen tC^O-strands, then introduce a five time excess of the unmodified strand

S_{unmod} (Table 3.1). The kinetics of the reaction is then followed as equilibrium settles and the majority of the tC^O labeled strands in the duplex gets competed out in to ssDNA form (Figure 3.3).

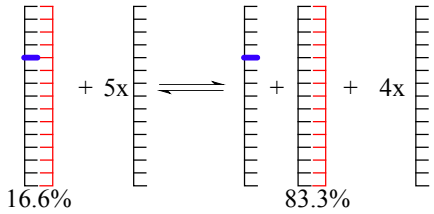

Figure 3.3: The DNA strand exchange reaction that is expected to occur. The ladder-like structures represent dsDNA and the comb-like structures represent ssDNA where the steps or comb tooths represent the DNA bases. The thicker blue line indicates the tC^O in one of S_1-S_8 strands and the red strand indicates the complementary strand S_{compl}.

It is evident that the theoretical equilibrium of the reaction in Figure 3.3 is that 5/6 or 83.3% of the labeled strands will be in ssDNA form (right side of the reaction) and 1/6 or 16.6% will remain in dsDNA form (left side of the reaction) at equilibrium. This assumption is true only if the binding constants (approximately T_m) of labeled and unlabeled ssDNA are the same. The large change from dsDNA-form to ssDNA-form for the labeled strand is considered large enough for detection.

It is desired to have a concentration of 0.5 μM of tC^O-strand in the measured samples with a total volume of 1 mL and a negligible dilution effect of 1.5% to the medium (here referreing to the different forms of PEG used) as the DNA was added.

A $dsDNA_{tC^O}$ stock for F_0-reference and part of the $F(t)$-kinetics trace sample was annealed in buffer using the chosen strands and yielding dsDNA concentration of 100 μM in 100 μL. Of these 5 μL is added to 985 μL medium at each measurement. The $ssDNA_{unmod}$ (S_{unmod}, Table 3.1) was diluted to 250 μM of which 10 μL was added to the 985 mL medium giving a 5 times excess of the single strand compared to the added $dsDNA_{tC^O}$ in the kinetics trace sample $F(t)$. The higher reference sample stock, F_∞, was prepared for 3 measurements by adding 15 μL of the 100 μM annealed $dsDNA_{tC^O}$ to 30 μL of the 250 μM of $ssDNA_{unmod}$ and re-annealed. In this way the reference samples become more reliable for the batch in use. Figure 3.4 below illustrates the whole procedure just described.

The fitting of the model, equation (2.8), to the first 300 min of the kinetics raw data and thereafter the inverted rate constants were determined using MATLAB R2010B.

3.4 The P2 C repressor project

The first step was to prepare the proper buffer and recheck the stock concentrations of the DNA single strands for this project (Table 3.2), as well as the concentration of the P2 C protein. Once the concentrations were under control, duplexes P_{unmod}:P_{comp} and P_2:P^*_{comp} were annealed. These were used to detect the binding

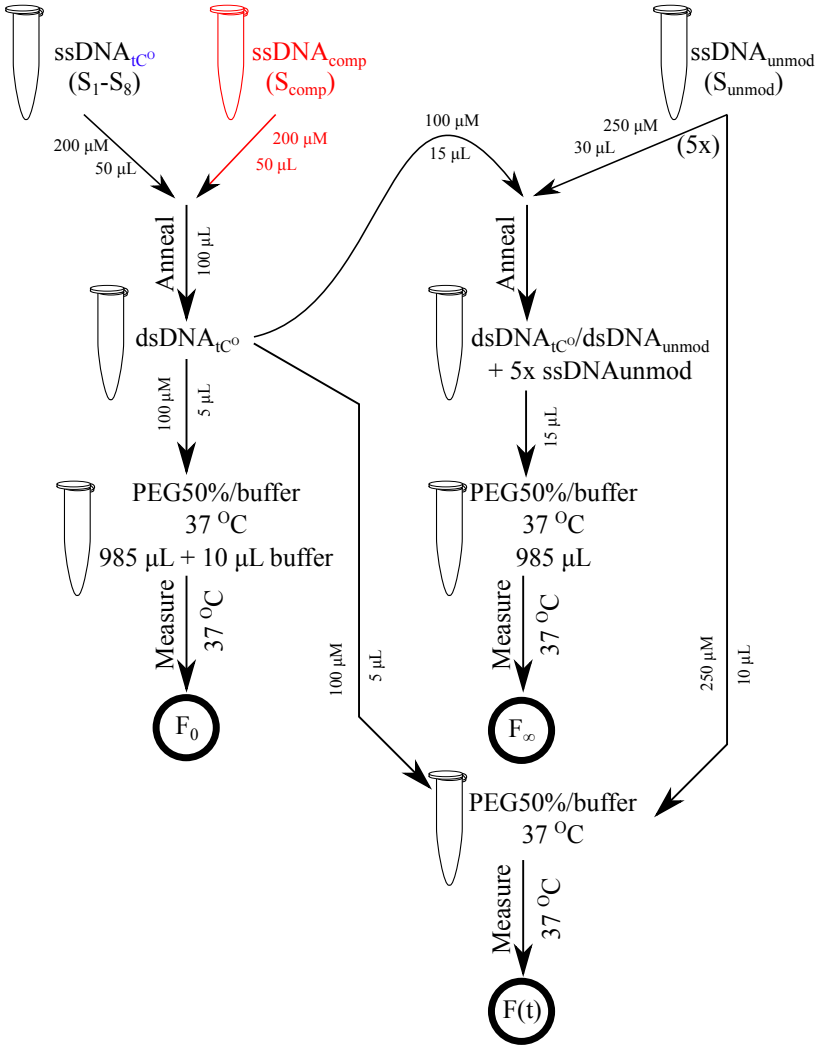

Figure 3.4: The illustrated experimental procedure of DNA strand exchange kinetics. The ssDNA$_{compl}$ (S$_{compl}$) and tC^O are colored for easier comparison with Figure 3.3.

of P2 C repressor to labeled and unlabeled DNA duplex using anisotropy from the tryptophan in the P2 C monomers. Further detection of the binding was also made using anisotropy from tC^O. Finally a titration of protein to a solution of DNA gave an initial estimate of the binding constant.

3.4.1 Buffer

A 1 L Tris-HCL buffer stock was prepared containing 150 mM NaCl and 37.5 mM Tris with pH adjusted to 7.5 using diluted HCl/NaOH. The solution was filtered through micropore filter (pore diameter 0.45 μm) and stored in several 50 mL TPP® tubes as a precautionary measure against contamination.

Upon usage the buffer stock was diluted with MilliQ-H_2O to 100 mM NaCl and 25 mM Tris.

3.4.2 P2 C repressor protein

The P2 C repressor was kindly supplied by Assistant Professor Pål Stenmark's group[3] in two forms; the wild-type (wt) form and the selenomethionine-labeled (seleno) form. The concentrations of the received proteins were estimated to 207.76 μM for the seleno and 254.68 μM for the wt using the extinction coefficient (ϵ_{280nm}) of 25 900 $M^{-1}cm^{-1}$ for the dimer. The molecular weight of the wt P2 C repressor dimer is 22 034 g/mol and for the slightly heavier seleno 22 503 g/mol, calculated with the help of the peptide sequence (Table 3.5). The presence of the firmly anchored fluorescent amino acid tryptophan makes it possible to do anisotropy measurements on the protein itself without any incorporated artificial probe.

The protein has been stored in a −80 °C refrigerator and constantly kept on ice during laboratory work.

Table 3.5: The peptide sequence for the P2 C monomer. Note the presence of tryptophan (W). The sequence is read from left to right across the 10-peptide columns.

Amino acid sequence		# of amino acids
MSNTISEKIV	LMRKSEYLSR	20
QQLADLTGVP	YGTLSYYESG	40
RSTPPTDVMM	NILQTPQFTK	60
YTL**W**FMTNQI	APESGQIAPA	80
LAHFGQNETT	SPHSGQKTG	99

3.4.3 Experimental procedure

After the concentrations of the P2 C repressor protein and the DNA strands (Table 3.2) were set, DNA duplexes P_{unmod}:P_{comp} and P_2:P^*_{comp} with 1% excess of the complementary strands were annealed to yield 200 μL 10 μM duplex stocks.

Anisotropy from tryptophan was first measured on the P2 C seleno and wt protein alone, at 20 μM and 16 μM, respectively. Further anisotropy measurements were preformed, in the presence of both modified (P_2:P^*_{comp}) and unmodified (P_{unmod}:P_{comp}) duplexes. The P2 C seleno protein concentration was 6.667 μM with the same concentration of modified and unmodified duplexes. The P2 C wt protein concentration was at 6.15 μM and concentration of modified and unmodified duplexes were also the same.

The same anisotropy measurement procedure was repeated but instead using tC^O as the probe with P2 C seleno and wt. The modified DNA duplex (P_2:P^*_{comp}) was used again but in the concentration 6.07 μM and the P2 C seleno protein at two times excess.

3. Center for Biomembrane Research, Department of Biochemistry and Biophysics, Stockholm University, SE-106 91 Stockholm, Sweden

In an attempt to determine the binding constant, a titration was performed of the P2 C seleno protein into a 2 μM 1000 μL modified dsDNA mixture (P_2:P^*_{comp}). The titration volume steps of the P2 C protein were between $0.75 - 1.5$ μL 207.758 μM to a total volume of 48.05 μL. For a full list of titrated amounts see Appendix 10.2 (Table 10.8)

3.5 Illustrations

The illustrations of DNA and RNA were generated in HyperChem and further esthetically modified in UCSF Chimera. The protein illustrations were obtained from RCSB PDB Protein Data bank and esthetically modified in Chimera. The Lewis structures presented are created using ChemDraw. All other illustrations or modifications to illustrations were made in Inkscape.

3.6 Calculations

All of the calculations made, such as finding T_m, fitting models to kinetics traces and deriving binding constant from binding curves were made using MATLAB R2010B. Fitting was preferably done in the MATLAB subprogram ”cftool”. The graphs were in most cases generated in Origin 6.

4 Results

This section contains the results acquired in the two different projects of this Thesis. They will be divided accordingly.

4.1 DNA strand exchange

From the measured melting temperatures of the dsDNA and the relative differences in emission between ssDNA and dsDNA forms, strands S_1, S_2, S_4 and S_5 were chosen for the DNA strand exchange project. The measured values and motivations are found in Table 4.1.

Table 4.1: The melting temperatures from the highest derivative point and the half-temperature method, where ΔT_m is the difference between the T_m of the unmodified- and modified duplexes. ΔEm is the emission difference between labeled ssDNA and dsDNA in percent. All emission measurements were performed in buffer at 22 °C. The reasons for choosing the strands is seen in column Motivation. The graphs of the respective melting temperature measurements (stage 3 & 4) are found in Appendix 10.1 as well as the different emission spectra for ssDNA and dsDNA (Figures 10.1 & 10.2).

	Derivative		Half temp.			
Strand label	$T_{m,\text{deriv}}$ [°C]	$\Delta T_{m,\text{deriv}}$ [°C]	$T_{m,\text{half}}$ [°C]	$\Delta T_{m,\text{half}}$ [°C]	ΔEm [%]	Motivation
S_{unmod}:S_{compl}	70.8	-	69.8	-	-	
S_1:S_{compl}	74.3	3.5	70.5	0.8	59.85	Deviating T_m, ok contrast
S_2:S_{compl}	71.3	0.5	70.3	0.5	67.77	Ok T_m, good contrast
S_3:S_{compl}	71.5	0.8	69.5	-0.3	73.16	
S_4:S_{compl}	71.3	0.5	69.5	-0.2	63.60	Good T_m, good contrast
S_5:S_{compl}	70.7	0.0	69.5	-0.2	91.10	Ok T_m, best contrast
S_6:S_{compl}	71.3	0.5	67.5	-2.3	41.68	
S_7:S_{compl}	71.7	1.0	67.5	-2.3	48.60	
S_8:S_{compl}	71.2	0.5	69.0	-0.8	34.00	

The kinetics measurements using the second best, S_5, were conducted in the different medias in the quest of finding the PEG which most efficiently enhanced the rate of strand exchange. The resulting kinetics traces are found in Figure 4.1. The inverted rate constants, using equation (2.8), for each of the traces are found in Table 4.2

Since PEG1000 and PEG150 displayed similar results to PEG6000 in overall reaction kinetics, focus was centered on comparison of the Na-phos. buffer-, PEG6000- and PEG178 kinetics. Figure 4.2 displays the main results for this part of the Thesis, namely the kinetics traces (combined with yields) for the S_4 dsDNA, the best representation for the unmodified DNA duplex, in the three media of interest. The corresponding inverted rate constants are found in Table 4.3.

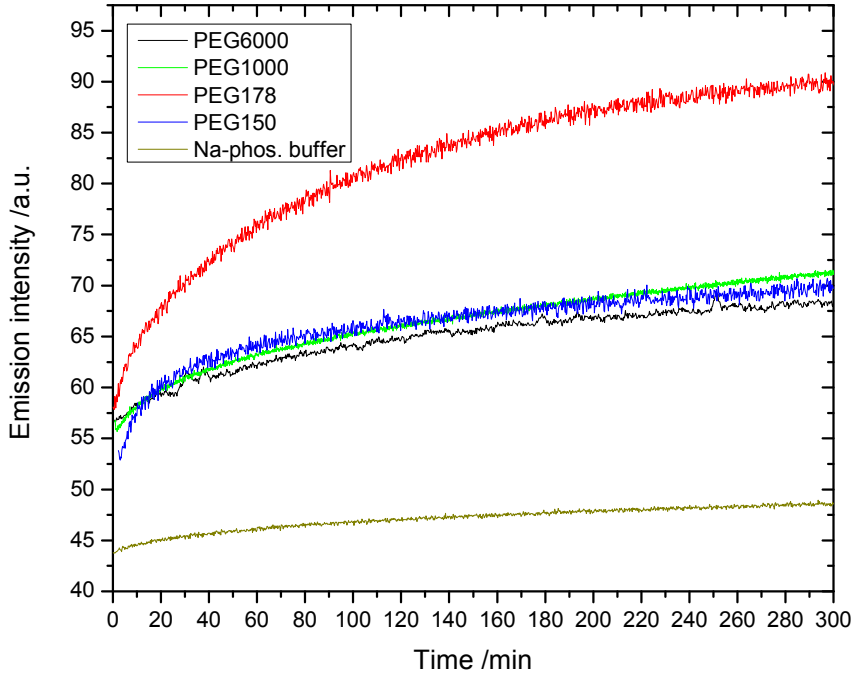

Figure 4.1: Kinetic traces of strand exchange for strand S_5 in the different PEGs (Table 3.4) and buffer. Measurements are preformed at 37 °C and ran for at least 300 min.

Table 4.2: The inverted rate constants of kinetics traces in Figure 4.1 with the corresponding r^2-values of the fit. More complete statistical information about the curve fitting is found in Table 10.2

Medium used	τ [s]	r^2
PEG6000	116.4	0.9881
PEG1000	143.4	0.9894
PEG178	92.3	0.9922
PEG150	71.04	0.9513
Na-phos. buffer	132	0.9836

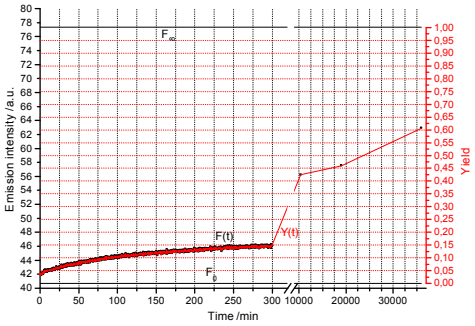

(a) S_4:S_{compl} duplex in Na-phos. buffer

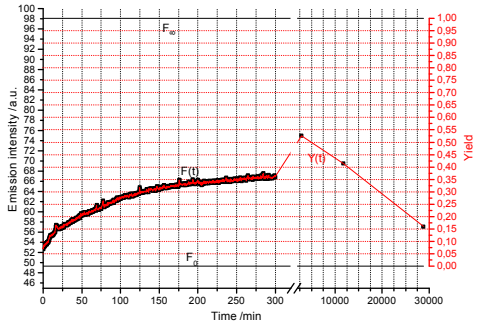

(b) S_4:S_{compl} duplex in PEG6000

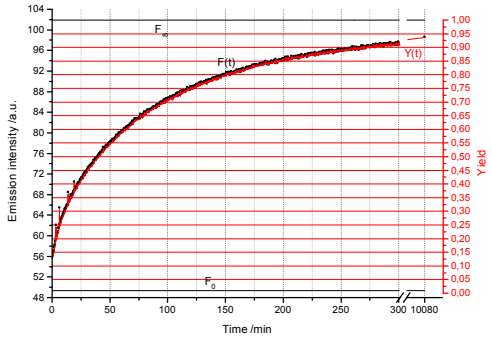

(c) S_4:S_{compl} duplex in PEG178

Figure 4.2: The main strand, S_4, in the three media of interest. The extended points are measured after longer storage in an incubation chamber at 37 °C. The traces for all four chosen strands in these media are found in Appendix 10.1 (Figure 10.3, 10.4 & 10.5) together with their rate constants in Tabels 10.4, 10.5 & 10.6.

Table 4.3: The inverted rate constants for kinetics traces using strand S_4 in Figure 4.2 with the corresponding r^2 of the fit. More complete statistical information about the curve fitting is found in Table 10.3 in Appendix 10.1.

Medium used	τ [s]	r^2	$\text{Yield}_{300\text{ min}}$ [%]
Na-Phos. buffer	129.2	0.9871	15
PEG6000	93.9	0.9961	37
PEG178	80.72	0.9961	92

4.2 Binding constant of P2 C repressor

The anisotropy of the P2 C protein using the intrinsic tryptophan was found to increase in both the seleno and wt form. The anisotropies are found in Table 4.4

Table 4.4: Anisotropy (r) of the P2 C protein measured using tryptophan, with and without the two duplexes P_2:P^*_{comp} and P_{unmod}:P_{comp}. The first row of anisotropy values corresponds to the free proteins without dsDNA present. The last two rows are anisotropies with the corresponding dsDNA present. The corresponding graphs are found in Appendix 10.2 (Figure 10.7).

dsDNA	P2 C wt	P2 C seleno
-	0.092	0.101
P_{unmod}:P_{comp}	0.145	0.153
P_2:P^*_{comp}	0.151	0.140

Further anisotropy measurements were made using tC^O in the DNA in presence of the P2 C seleno and wt protein. Also here an increase of anisotropy was observed, as seen in Table 4.5.

Table 4.5: Anisotropy (r) of the $dsDNA_{P_2:P^*_{comp}}$ using tC^O in the presence of P2 C seleno and wt protein. The corresponding graphs are found in Appendix 10.2 (Figure 10.6).

	$dsDNA_{P_2:P^*_{comp}}$	$dsDNA_{P_2:P^*_{comp}}$ and P2 C wt	$dsDNA_{P_2:P^*_{comp}}$ and P2 C seleno
r	0.267	0.289	0.297

From these anisotropy investigations it was concluded that the P2 C protein binds to DNA and we moved on to perform a first actual titration to find an estimate of the binding constant. The titration curve is shown in Figure 4.3 and the statistics of the fitting of equation (2.7) to the titration data is given in Table 4.6.

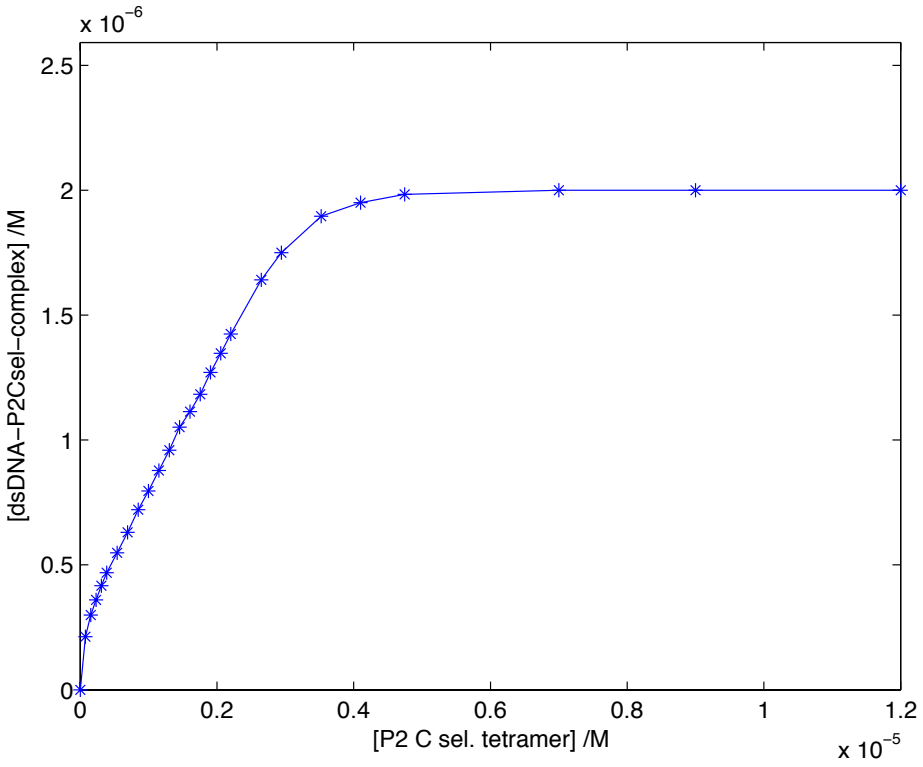

Figure 4.3: The titration curve of the P2 C seleno protein in to a solution of $dsDNA_{P_2:P^*_{comp}}$. The stars mark the titration points, the line is just a guide for the eye. Since non-cooperativity is assumed between the two P2 C repressor dimers, it is considered that one P2 C tetramer binds to one DNA duplex (Figure 2.10b). For a full list of titrated amounts see Appendix 10.2 (Table 10.8).

Table 4.6: Binding constant K of the P2 C seleno protein and dsDNA-titration together with the corresponding statistics of the fitting of equation (2.8). The constant c is the total $dsDNA_{P_2:P^*_{comp}}$ concentration at the beginning of the titration and therefore also maximum possible complex concentration at the end.

K $[M^{-1}]$	c [M]	r^2	SSE	RMSE
6e7 (2.684e7, 9.316e7)	2e-6 (1.965e-6, 2.035e-6)	0.998	2.394e-14	3.159e-8

5 Discussion

This section will cover interpretation of the results as well as their sources of errors.

5.1 DNA strand exchange

The initial objective of this project was to investigate if the findings done by Feng *et al.* [6] could be repeated using DNA strands of different lengths and utilizing other fluorescent labels. From the study by Feng *et al.* we expected to reach a strand exchange equilibrium within 300 min with a significantly higher rate constant k (equation 2.9) than in buffer.

The choice of most suitable strands for this experiment (Table 4.1) was based on data from melting temperatures and emission properties in ssDNA- and dsDNA-form. However, this was only done in buffer and it is not obvious that the choices had been the same if the selection procedure had included the melting temperatures and emission properties in PEG as well. If this improved selection process was to be performed, one would face a problem. In the previous study by Feng *et al.* [6] PEG has been observed to have a "thermal memory". This means that if a melting temperature experiment is conducted in PEG, the effects of the first heat-and-cool-stage would change the environment for the DNA in the second heat-and-cool-stage hence compromising the results.

Since the kinetics using PEG6000 did not show as high strand exchange efficiency nor as high reaction yield as expected after 300 min, a search for more efficient PEGs began. Since S_5 has the best emission contrast we chose that strand to find good PEG-solutions. A series of different PEGs were tested (Figure 4.1) and two of them (PEG1000 & PEG150) showed similar overall trends in kinetics as PEG6000 and, hence, we did not use those PEGs further. PEG178 showed great promise as the kinetics trace nearly reached the equilibrium value within 300 min (Figure 10.5) and its rate constant was higher than in most of the other PEGs.

It should be noted that the rate constant, in combination with the yield, represents the strand exchange efficiency, or in other words, the higher the k ($1/\tau$) the quicker the kinetics traces flatten out. However, when analyzing the data in this way we do not take into consideration the fact that most of these curves are very far from reaching 100% reaction yield.

As work advanced, kinetics traces of all four chosen strands (S_1, S_2, S_4 & S_5) were recorded in the three chosen media (Na-phos. buffer, PEG6000 & PEG178). Kinetics for the the strand having properties closest to the native ones, S_4 (Figure 4.2), displayed highest τ in buffer (Table 4.3), followed by PEG6000 and PEG178. This is reasonable considering that the kinetics yields increases in that order. All kinetics samples were stored in incubation chamber (37 °C) for at least 2 days and remeasured at least once to give a long-term kinetics trend. As seen for strand S_4 in Figure 4.2, all trends initially point upwards, more for Na-phos. buffer and PEG6000 than for PEG178. This is expected as the PEG178-sample is close to equilibrium already

after 300 min. However, after several days of storage at 37 °C, the Na-phos. buffer-sample still indicate an increasing trend in yield while the trend drops for PEG6000-sample. The reason for this is yet unknown but we suspect that the DNA-structure is seriously perturbed since we find that the DNA absorption gets new features and, moreover, the absorption maximum is increased (data not shown).

The individual results for all four strands in all three buffers are found in Appendix 10.1 (Figure 10.3, 10.4 & 10.5) together with their inverted rate constants in Tables 10.4, 10.5 & 10.6. The general trends in each medium are similar. However, strand S_5 shows somewhat higher yield in the two different PEGs, which is expected due to its slight destabilized duplex. A puzzling observation is that the over-stabilized strand S_1 produces the highest yield in Na-phos. buffer and on average is similar to S_2 & S_4 in the two PEG media.

The main difference between PEG6000 and PEG178 is the size and hence the number of molecules present in each of the mixtures. PEG6000 gives higher crowding effect than PEG178 due to the larger size and higher weight. PEG178 destabilizes the DNA duplex more as it makes the DNA environment more hydrophobic and thus lowers the T_m of dsDNA (Punton, A - personal contact) [55].

5.2 Binding constant of P2 C repressor

The anisotropy measurements of the P2 C repressor using tryptophan gave an increase in anisotropy of roughly 50% between pure protein and protein in presence of dsDNA. This is true for both the wt and the seleno P2 C repressor (Table 4.4).

Anisotropy using tC^O gave only a slight increase (8-11%) upon dsDNA binding to the seleno and wt P2 C repressor (Table 4.5). One possible explanation to this minor increase could be that the dsDNA structure is destabilized on the binding site of the protein, thus making the environment of tC^O less restrictive to movement. It should also be noted that an anisotropy of 0.3 is high and that a further increase might be difficult to detect.

The FRET titration curve was measured using the same seleno P2 C repressor-tube as for the tC^O-anisotropy measurements. This tube unfortunately ran out at approximately 1.98 μM concentration of the P2 C seleno tetramer (Figure 4.3). In order to have enough data for fitting the model, equation (2.7), the last three points (the most spread ones) were fabricated to represent the expected linear trend in that area. The points were designed by taking half of the height-difference between the two last measured points and adding that to the height of the last measured point. The fabricated points were positioned far away from the last measured point and with a wide spread in between. See Appendix 10.2 for the full titration (Table 10.8) as well as the calculation of the last three points. This is a rather unorthodox approach for achieving results but it can be justified as this was an initial titration with the purpose of giving a first guess on the magnitude of the binding constant. The main information about the binding constant is in the curved region of the binding titration and the fabricated values are outside of that area.

A peculiar deviation in the binding curve (Figure 4.3) is found in the beginning, in the large slope from origo to the first titration point. The reason behind this deviation is yet to be explained but it required the binding model, equation (2.7), to be tweaked somewhat in order to fit it better to the raw data. The model was allowed to be positioned so that the y-axis intercept was > 0. This is also a bit unorthodox as the binding constant expression, equation 2.3, is defined so that there is no complex formed if no protein is added. The modifications to the model break this definition.

From Figure 4.3 we find that approximately 2.5 P2 C repressor dimers are needed to saturate the DNA. In previous investigations in Stenmark's lab it has been suggested that 2 dimers *i.e.* a tetramer is needed to saturate the binding sites on DNA. In light of those results our findings here are somewhat puzzling.

As it turned out later, the stock concentrations of the protein used in these specific anisotropy measurement and the titration was in fact lower than first estimated, thus there is a possibility that the anisotropy difference between bound and unbound dsDNA to P2 C repressor is even larger at full saturation. The titration has been redone by Ph.D. student Anke Dierckx under better control of the concentrations and the expected saturation at 2 P2C repressor dimers : 1 dsDNA was observed. The trend of the titration does however support the assumed simplification of non-cooperativity, as explained in Figure 2.13.

6 Future work

Regarding the DNA strand exchange project one interesting thing to do, for the sake of comparison with Feng *et.al*, would be to use the very same sequences with tC^Oas label, and the sequences from this Thesis with their DNA-labels. This would expose any differences regarding the different labels and strands, and hence ease the comparison.

Even though PEG has been observed to have some sort of thermal memory it was still originally planned to conduct melting temperature experiments in PEG but due to time limitations that was left out. I believe it would still be interesting to do the melting temperature experiments and maybe compare the results with the DNA that rested in incubation chamber at 37 °C and se if there are similarities, if any, to the DNA decay observed in the incubated samples. Another thing that was disregarded due to time limitations was a more thorough examination of the kinetics in PEG1000 and PEG150. Especially PEG150 displayed a surprisingly low τ but did similarly as PEG6000 in terms of kinetics emission.

In terms of dsDNA stability it would have been interesting to do circular dichroism (CD) measurements on the kinetics samples to investigate if the dsDNA still remains in its normal B-form. Consequently a CD measurement would also be done on the PEG6000 samples where clearly something happened to the DNA after some time in storage at 37 °C.

The P2 C repressor binding was well detected using FRET. It would however be interesting to investigate the rapid increase in detection of the first titration step. It would be advisable to take as small steps of titration as possible in the beginning to get a higher resolution of the anomaly. Further, as the bending of the binding curve is very important for the determination of the binding constant, it would be good to also there take as small titration steps as possible. Two ways of further confirming the binding curve would be to run anisotropy measurements using tC^O and/or tryptophan during a titration. Although this may be very time-consuming work, it would probably be worth the effort.

Another interesting thing would be to investigate the structure of the dsDNA that is bound to the P2C repressors. This can also be done using FRET but would require many more labeled DNA strands than used in this project. The data from these experiments could then be used to determine both the bending and possible twisting of the DNA duplex.

7 Conclusions

For the DNA strand exchange project it can be concluded that the different forms of PEG in all cases increased the reaction yield compared to Na-phos. buffer alone. Highest yield obtained within the kinetics trace measurement was in PEG178 as well as the highest strand exchange efficiency (k) followed by PEG6000 and Na-phos. buffer, in that order. The trends in kinetics and yields did not completely follow the hypothesis based on the strands thermal stability that strands with highest T_m would strand exchange slower than those with lower T_m. There are probably more factors influencing strand exchange than thermal stability of the strands, for example the functional groups and length of the crowding agent.

The binding constant of P2 C repressor to dsDNA could be determined using tC^O-tC_{nitro} FRET-pair as probes in DNA duplex. An initial estimate of at the binding constant is $6 \cdot 10^7$ M^{-1} based on the first successful titration. Anisotropy with regard to the tryptophan in P2 C repressor can be used to detect binding to dsDNA with a dynamic range of $\geq 50\%$ of free P2 C repressor anisotropy. An anisotropy change is also detectable using tC^O as P2C repressor binds, although with a dynamic range of 8-11% of free tC^O-tC_{nitro}-labeled DNA duplex.

8 Acknowledgements

First of all I would like to thank my main supervisor Marcus Wilhelmsson for allowing me to do my Thesis in your group. Your excellent supervision is much appreciated, as is your humor and positive thinking. Another very important person is my co-supervisor Fredrik Westerlund. Thank you so much for the invaluable guidance in the DNA strand exchange project. Thank you both for your never-ending curiosity and energy, especially during the last few intense weeks. You are both true inspirations!

Anke Dierckx and Bobo Feng, thank you both for all your help, both theoretical and practical, throughout my Thesis. It would not have been the same without you.

My beloved fiancé, Maria Matson, thank you for your understanding and continuous support, both in good and bad times. I love you so much!

I would also like to thank everyone at the division of Physical Chemistry for making me feel welcome and creating a great working environment.

Last but absolutely not least, to family and friends, thank you all!

9 References

[1] Madigan, M. and Martinko, J. [2006] *Brock Biology of Microorganisms*. Pearson Prentice Hall, Upper Saddle River, NJ 07458, eleventh edition.

[2] Benson, F.; Stasiak, A.; and West, S. [1994] Purification and characterization of the human Rad51 protein, an analogue of E.coli RecA. *The EMBO journal*, **13**(23), 5764.

[3] Lusetti, S. and Cox, M. [2002] The bacterial RecA protein and the recombinational DNA repair of stalled replication forks. *Annu. Rev. Biochem.*, **71**(1), 71–100.

[4] Sehorn, M.; Sigurdsson, S.; Bussen, W.; Unger, V.; and Sung, P. [2004] Human meiotic recombinase Dmc1 promotes ATP-dependent homologous DNA strand exchange. *Nature*, **429**(6990), 433–437.

[5] Seitz, E.; Brockman, J.; Sandler, S.; Clark, A.; and Kowalczykowski, S. [1998] RadA protein is an archaeal RecA protein homolog that catalyzes DNA strand exchange. *Genes & development*, **12**(9), 1248.

[6] Feng, B.; Frykholm, K.; Nordén, B.; and Westerlund, F. [2010] DNA strand exchange catalyzed by molecular crowding in PEG solutions. *Chem. Commun.*, **46**(43), 8231–8233.

[7] Sandin, P.; Borjesson, K.; Li, H.; Martensson, J.; Brown, T.; Wilhelmsson, L. M.; and Albinsson, B. [2008] Characterization and use of an unprecedentedly bright and structurally non-perturbing fluorescent DNA base analogue. *Nucleic Acids Res.*, **36**(1), 157.

[8] Massad, T.; Skaar, K.; Nilsson, H.; Damberg, P.; Henriksson-Peltola, P.; Haggard-Ljungquist, E.; Hogbom, M.; and Stenmark, P. [2010] Crystal structure of the P2 C-repressor: a binder of non-palindromic direct DNA repeats. *Nucleic Acids Res.*, **38**(21), 7778–7790.

[9] Crick, F. [1970] Central dogma of molecular biology. *Nature*, **227**(5258), 561–563.

[10] Watson, J. and Crick, F. [1953] A structure for deoxyribose nucleic acid. *Nature*, **171**, 737–738.

[11] Petersheim, M. and Turner, D. [1983] Base-stacking and base-pairing contributions to helix stability: thermodynamics of double-helix formation with CCGG, CCGGp, CCGGAp, ACCGGp, CCGGUp, and ACCGGUp. *Biochemistry*, **22**(2), 256–263.

[12] Yakovchuk, P.; Protozanova, E.; and Frank-Kamenetskii, M. [2006] Base-stacking and base-pairing contributions into thermal stability of the DNA double helix. *Nucleic Acids Res.*, **34**(2), 564.

[13] Bloomfield, V.; Crothers, D.; and Tinoco, I. [2000] *Nucleic acids: structures, properties, and functions*. Univ Science Books.

[14] Hutton, J. [1977] Renaturation kinetics and thermal stability of DNA in aqueous solutions of formamide and urea. *Nucleic Acids Res.*, **4**(10), 3537–3555.

[15] Protozanova, E.; Yakovchuk, P.; and Frank-Kamenetskii, M. [2004] Stacked-unstacked equilibrium at the nick site of DNA. *J. Mol. Biol.*, **342**(3), 775–785.

[16] Sen, A. and Nielsen, P. [2007] On the stability of peptide nucleic acid duplexes in the presence of organic solvents. *Nucleic Acids Res.*, **35**(10), 3367.

[17] Sen, A. and Nielsen, P. [2009] Hydrogen bonding versus stacking stabilization by modified nucleobases incorporated in PNA· DNA duplexes. *Biophys. Chem.*, **141**(1), 29–33.

[18] Anastassopoulou, J. and Theophanides, T. [2002] Magnesium-DNA interactions and the possible relation of magnesium to carcinogenesis. Irradiation and free radicals. *Critical reviews in oncology/hematology*, **42**(1), 79–91.

[19] Liu, J.; Zhang, T.; Lu, T.; Qu, L.; Zhou, H.; Zhang, Q.; and Ji, L. [2002] DNA-binding and cleavage studies of macrocyclic copper (II) complexes. *J. Inorg. Biochem.*, **91**(1), 269–276.

[20] Reymer, A.; Frykholm, K.; Morimatsu, K.; Takahashi, M.; and Nordén, B. [2009] Structure of human Rad51 protein filament from molecular modeling and site-specific linear dichroism

spectroscopy. *Proceedings of the National Academy of Sciences*, **106**(32), 13 248.

[21] Chen, Z.; Yang, H.; and Pavletich, N. [2008] Mechanism of homologous recombination from the RecA–ssDNA/dsDNA structures. *Nature*, **453**(7194), 489–494.

[22] Selmane, T.; Wittung-Stafshede, P.; Maraboeuf, F.; Voloshin, O.; Nordén, B.; Camerini-Otero, D.; and Takahashi, M. [1999] The L2 loop peptide of RecA stiffens and restricts base motions of single-stranded DNA similar to the intact protein1. *FEBS Lett.*, **446**(1), 30–34.

[23] Tajima, K.; Kim, W.; Akaike, T.; and Maruyama, A. [2002] Acceleration of DNA strand exchange reaction by cationic polymers. *Nucleic acids symposium series*, **2**(1), 265.

[24] Kim, W.; Sato, Y.; Akaike, T.; and Maruyama, A. [2003] Cationic comb-type copolymers for DNA analysis. *Nat. Mater.*, **2**(12), 815–820.

[25] Kim, W.; Akaike, T.; and Maruyama, A. [2002] DNA strand exchange stimulated by spontaneous complex formation with cationic comb-type copolymer. *J. Am. Chem. Soc.*, **124**(43), 12 676–12 677.

[26] Frykholm, K.; Bombelli, F.; Nordén, B.; and Westerlund, F. [2008] Enhanced DNA strand exchange on positively charged liposomes. *Soft Matter*, **4**(12), 2500–2506.

[27] Frykholm, K.; Nordén, B.; and Westerlund, F. [2009] Mechanism of DNA Strand Exchange at Liposome Surfaces Investigated Using Mismatched DNA. *Langmuir*, **25**(3), 1606–1611.

[28] Ellis, R. [2001] Macromolecular crowding: obvious but underappreciated. *Trends Biochem. Sci*, **26**(10), 597–604.

[29] Minton, A. [2006] How can biochemical reactions within cells differ from those in test tubes? *J. Cell Sci.*, **119**(14), 2863.

[30] Minton, A. [2000] Implications of macromolecular crowding for protein assembly. *Curr. Opin. Struct. Biol.*, **10**(1), 34–39.

[31] Lukacs, G.; Haggie, P.; Seksek, O.; Lechardeur, D.; Freedman, N.; and Verkman, A. [2000] Size-dependent DNA mobility in cytoplasm and nucleus. *J. Biol. Chem.*, **275**(3), 1625.

[32] Han, J. and Herzfeld, J. [1993] Macromolecular diffusion in crowded solutions. *Biophys. J.*, **65**(3), 1155–1161.

[33] L
"usse, S. and Arnold, K. [1996] The interaction of poly (ethylene glycol) with water studied by 1h and 2h nmr relaxation time measurements. *Macromolecules*, **29**(12), 4251–4257.

[34] Rajulu, A. and Sab, P. [1996] Ultrasonic studies of water/poly (ethylene glycol) mixtures. *Eur. Polym. J.*, **32**(2), 267–268.

[35] Graham, N. and Chen, C. [1993] Interaction of poly (ethylene oxide) with solvent–5. the densities of water/poly (ethylene glycol) mixtures. *Eur. Polym. J.*, **29**(2-3), 149–151.

[36] Spink, C. and Chaires, J. [1995] Selective stabilization of triplex dna by poly (ethylene glycols). *J. Am. Chem. Soc.*, **117**(51), 12 887–12 888.

[37] Ninni, L.; Camargo, M.; and Meirelles, A. [1999] Water activity in poly (ethylene glycol) aqueous solutions. *Thermochim. Acta*, **328**(1-2), 169–176.

[38] Williams, A.; Wernette, C.; and Kaguni, L. [1993] Processivity of mitochondrial DNA polymerase from Drosophila embryos. Effects of reaction conditions and enzyme purity. *J. Biol. Chem.*, **268**(33), 24 855.

[39] Onidas, D.; Markovitsi, D.; Marguet, S.; Sharonov, A.; and Gustavsson, T. [2002] Fluorescence properties of DNA nucleosides and nucleotides: a refined steady-state and femtosecond investigation. *J. Phys. Chem. B*, **106**(43), 11 367–11 374.

[40] Wilhelmsson, L. M. [2010] Fluorescent nucleic acid base analogues. *Q. Rev. Biophys.*, **43**(02), 159–183.

[41] Ward, D. C.; Reich, E.; and Stryer, L. [1969] Fluorescence studies of nucleotides and polynu-

cleotides. I. Formycin, 2-aminopurine riboside, 2, 6-diaminopurine riboside, and their derivatives. *J. Biol. Chem.*, **244**(5), 1228–1237.

[42] Gilbert, S.; Stoddard, C.; Wise, S.; and Batey, R. [2006] Thermodynamic and kinetic characterization of ligand binding to the purine riboswitch aptamer domain. *J. Mol. Biol.*, **359**(3), 754–768.

[43] Lemay, J. F.; Penedo, J. C.; Tremblay, R.; Lilley, D. M. J.; and Lafontaine, D. A. [2006] Folding of the adenine riboswitch. *Chemistry & Biology*, **13**(8), 857–868.

[44] Hawkins, M. E.; Pfieiderer, W.; Mazumder, A.; Pommier, Y. G.; and Balis, F. M. [1995] Incorporation of a fluorescent guanosine analog into olignoucleotides and its application to a real time assay for the HIV-1 integrase 3'-Processing reaction. *Nucleic Acids Res.*, **23**(15), 2872.

[45] Hawkins, M. E. [2001] Fluorescent pteridine nucleoside analogs. *Cell Biochem. Biophys.*, **34**(2), 257–281.

[46] Lin, K.; Jones, R.; and Matteucci, M. [1995] Tricyclic 2'-deoxycytidine analogs: syntheses and incorporation into oligodeoxynucleotides which have enhanced binding to complementary RNA. *J. Am. Chem. Soc.*, **117**(13), 3873–3874.

[47] Wilhelmsson, L. M.; Holmen, A.; Lincoln, P.; Nielsen, P. E.; and Nordén, B. [2001] A Highly Fluorescent DNA Base Analogue that Forms Watson- Crick Base Pairs with Guanine. *J. Am. Chem. Soc*, **123**(10), 2434–2435.

[48] Börjesson, K.; Preus, S.; El-Sagheer, A. H.; Brown, T.; Albinsson, B.; and Wilhelmsson, L. M. [2009] Nucleic acid base analog FRET-pair facilitating detailed structural measurements in nucleic acid containing systems. *J. Am. Chem. Soc.*, **131**(12), 4288–4293.

[49] Preus, S.; Börjesson, K.; Kilså, K.; Albinsson, B.; and Wilhelmsson, L. M. [2009] Characterization of nucleobase analogue FRET acceptor tCnitro. *J. Phys. Chem. B*, **114**(2), 1050–1056.

[50] Mathews, C. K.; Van Holde, K. E.; and Aherm, K. G. [2000] *Biochemistry*. Addison Wesley Longman, 1301 Sansome Street, San Francisco, CA 94111, third edition.

[51] Ahlgren-Berg, A.; Henriksson-Peltola, P.; Sehlén, W.; and Haggård-Ljungquist, E. [2007] A comparison of the DNA binding and bending capacities and the oligomeric states of the immunity repressors of heteroimmune coliphages P2 and WΦ. *Nucleic Acids Res.*, **35**(10), 3167.

[52] Förster, T. [1948] Zwischenmolekulare energiewanderung und fluoreszenz. *Ann. Phys.*, **437**(1-2), 55–75.

[53] Lakowicz, J. R. [2006] *Principles of Fluorescence Spectroscopy*. Springer Science, Springer Science+Business Media, LLC, 233 Spring Street, New York, NY 10013, USA), third edition.

[54] Preus, S. [2009] *Fluorescent Nucleobase Analogues - Characterization And Uses*. Master's thesis, University of Copenhagen.

[55] Punton, A. [2011] PEG as a Catalyst in DNA Strand Exchange.

10 Appendix

10.1 DNA strand exchange

Table 10.1: DNA strands for DNA strand exchange project with both their production names and labels for easier reference. The position of the used base analogue tC^O is indicated by **X** in the 38 monomer long DNA sequences and the calculated extinction coefficiens at 260 nm are found in the rightmost column.

Strand name	Strand label	DNA sequences (38-mer)	ϵ_{260nm} [M^{-1} cm^{-1}]
A9371	S_1	5'-CCT **X**AC ACA CAT GCA GAG AGA GAG TGC ACA CAC ACA CC-3'	388 710
A9372	S_2	5'-CCT CA**X** ACA CAT GCA GAG AGA GAG TGC ACA CAC ACA CC-3'	388 710
A9373	S_3	5'-CCT CAC A**X**A CAT GCA GAG AGA GAG TGC ACA CAC ACA CC-3'	388 710
A9374	S_4	5'-CCT CAC ACA **X**AT GCA GAG AGA GAG TGC ACA CAC ACA CC-3'	388 710
A9375	S_5	5'-CCT CAC ACA CAT GCA GAG AGA GAG TGC A**X**A CAC ACA CC-3'	388 710
A9376	S_6	5'-CCT CAC ACA CAT GCA GAG AGA GAG TGC ACA **X**AC ACA CC-3'	388 710
A9377	S_7	5'-CCT CAC ACA CAT GCA GAG AGA GAG TGC ACA CA**X** ACA CC-3'	388 710
A9378	S_8	5'-CCT CAC ACA CAT GCA GAG AGA GAG TGC ACA CAC A**X**A CC-3'	388 710
B0080	S_{unmod}	5'-CCT CAC ACA CAT GCA GAG AGA GAG TGC ACA CAC ACA CC-3'	385 470
A9357	S_{unmod}	5'-CCT CAC ACA CAT GCA GAG AGA GAG TGC ACA CAC ACA CC-3'	385 470
A9358	S_{compl}	3'-GGA GTG TGT GTA CGT CTC TCT CTC ACG TGT GTG TGT GG-5'	353 790

Table 10.2: A more complete statistical summary of the curve fitting for kinetic traces using strand S_5. The coefficients of equation (2.8) are given with their respective with 95% confidence bounds within ()-brackets.

Medium used with S_5	F^*_∞ [a.u.]	ΔF [a.u.]	τ [s]	r^2	SSE	RMSE
PEG6000	68.94 (68.87, 69.02)	11.62 (11.55, 11.68)	114.3 (112.3, 116.3)	0.9918	82.55	0.2662
PEG1000	72.63 (72.54, 72.73)	14.98 (14.91, 15.06)	143.4 (141.2, 145.6)	0.9894	424.1	0.3766
PEG178	90.61 (90.49, 90.74)	29.19 (29.05, 29.34)	92.24 (90.87, 93.61)	0.9922	535.4	0.6688
PEG150	69.22 (69.13, 69.32)	12.92 (12.74, 13.1)	71.04 (68.7, 73.39)	0.9513	615.3	0.7191
Na-Phos. buffer	48.94 (48.89, 48.99)	4.597 (4.556, 4.638)	132 (128.3, 135.7)	0.9836	26.2	0.1479

Table 10.3: A more complete statistical summary of the curve fitting for kinetic tranes using strand S_4 (Figure 4.2). The coefficients of equation (2.8) are given with their respective with 95% confidence bounds within ()-brackets.

Medium used with S_4	F^*_∞ [a.u.]	ΔF [a.u.]	τ [s]	r^2	SSE	RMSE	$Yield_{300\ min}$ [%]
Na-Phos. buffer	46.41 (46.37, 46.45)	4.19 (4.157, 4.222)	129.2 (126, 132.3)	0.9871	17.26	0.12	15
PEG6000	67.35 (67.31, 67.4)	13.8 (13.75, 13.85)	93.9 (92.91, 94.9)	0.9961	55.85	0.2189	37
PEG178	97.6 (97.51, 97.7)	37.43 (37.29, 37.56)	80.72 (79.94, 81.5)	0.9961	427.3	0.5982	92

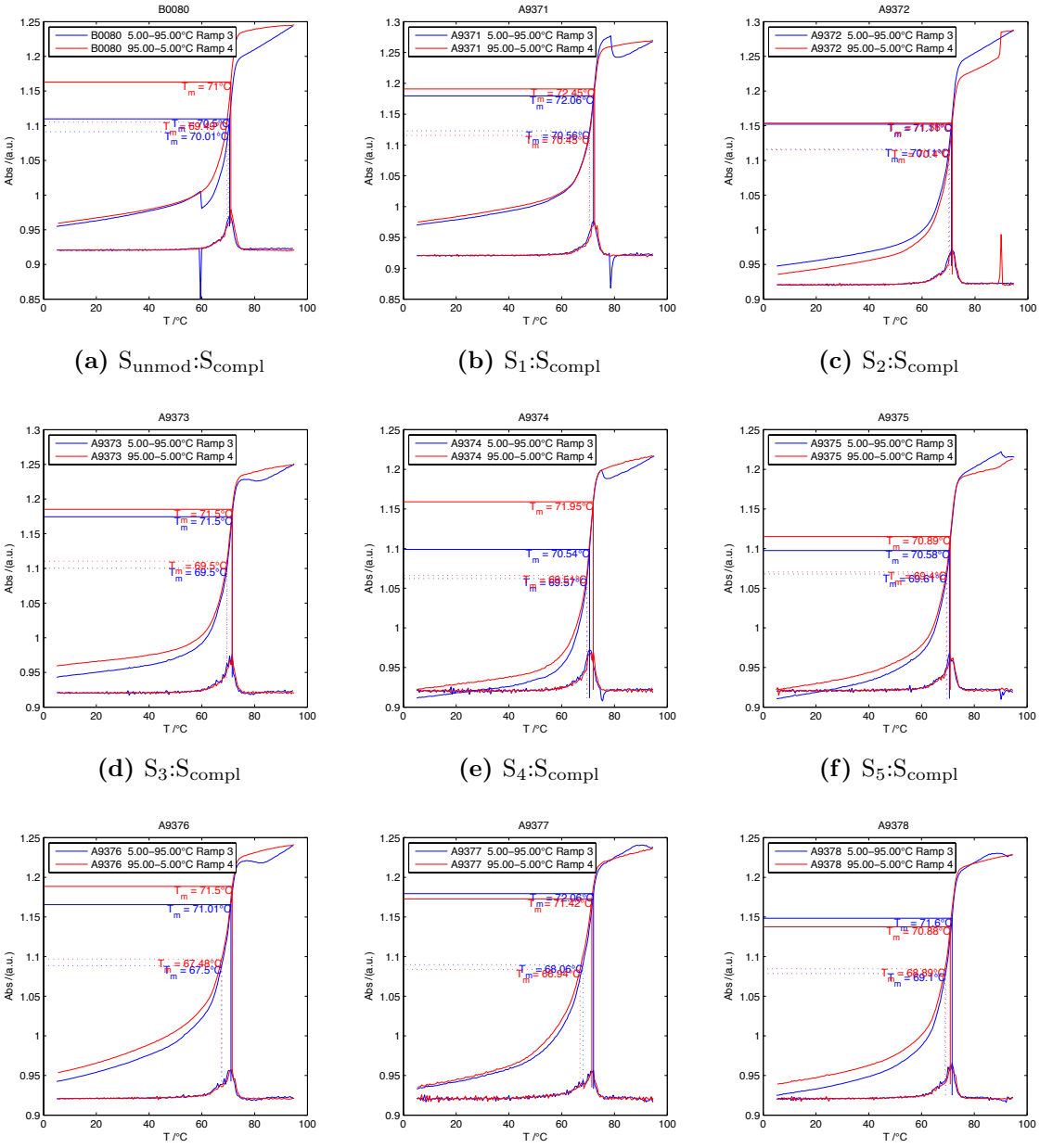

(a) S_{unmod}:S_{compl} **(b)** S_1:S_{compl} **(c)** S_2:S_{compl}

(d) S_3:S_{compl} **(e)** S_4:S_{compl} **(f)** S_5:S_{compl}

(g) S_6:S_{compl} **(h)** S_7:S_{compl} **(i)** S_8:S_{compl}

Figure 10.1: Graphs of the melting temperatures (ramp 3 & 4 is stage 3 & 4) used for choosing the proper strands for DNA strand exchange. The dotted straight lines indicate the $T_{m,\mathrm{half}}$ and the and the continuous lines indicate $T_{m,\mathrm{deriv}}$. The curves at the bottom of the graphs indicate the state of the derivative for the whole melting curves.

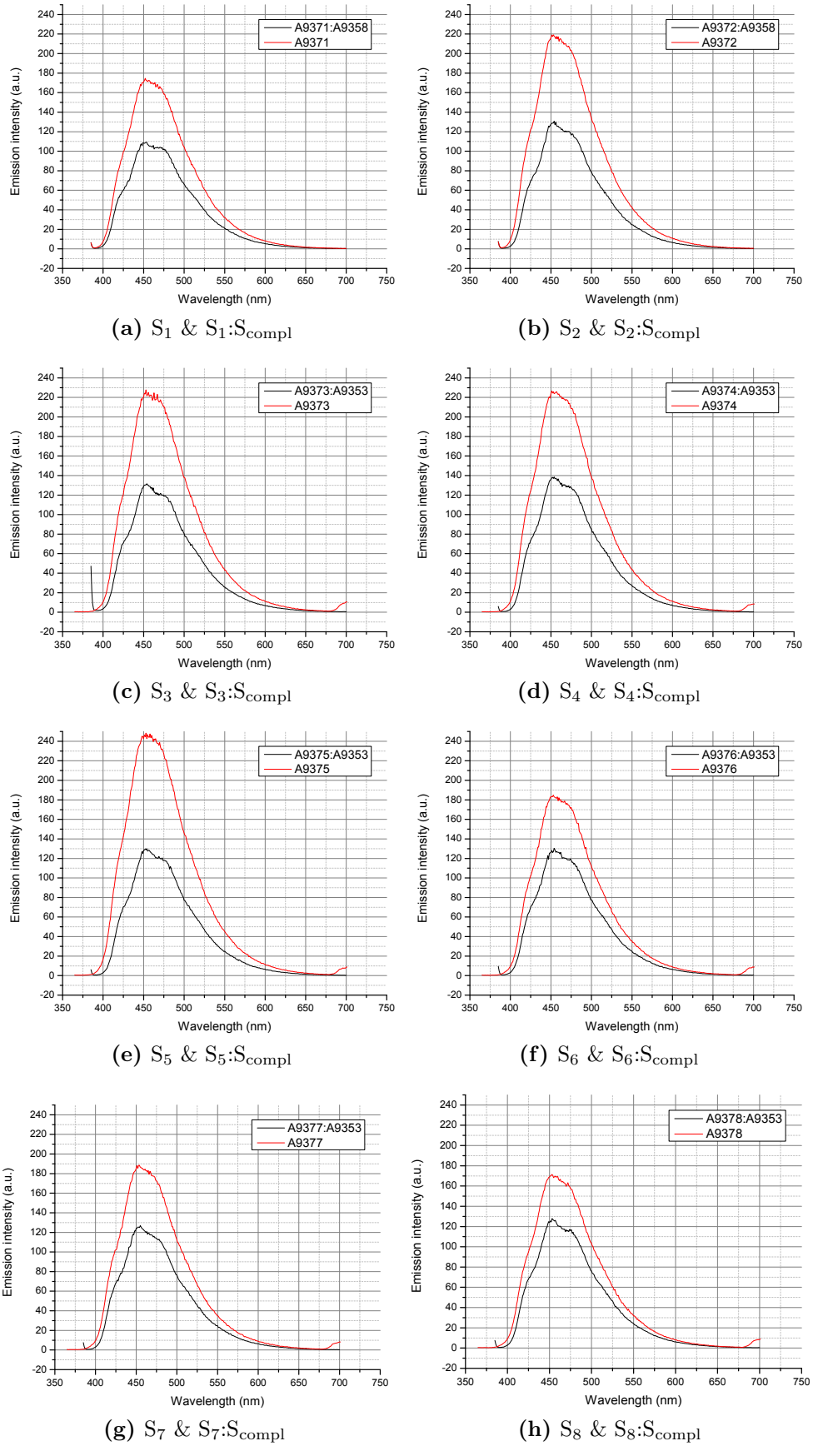

(a) S_1 & S_1:S_{compl} **(b)** S_2 & S_2:S_{compl}

(c) S_3 & S_3:S_{compl} **(d)** S_4 & S_4:S_{compl}

(e) S_5 & S_5:S_{compl} **(f)** S_6 & S_6:S_{compl}

(g) S_7 & S_7:S_{compl} **(h)** S_8 & S_8:S_{compl}

Figure 10.2: Emission graphs of ssDNA and dsDNA. Used for choosing the proper strands for the DNA strand exchange project.

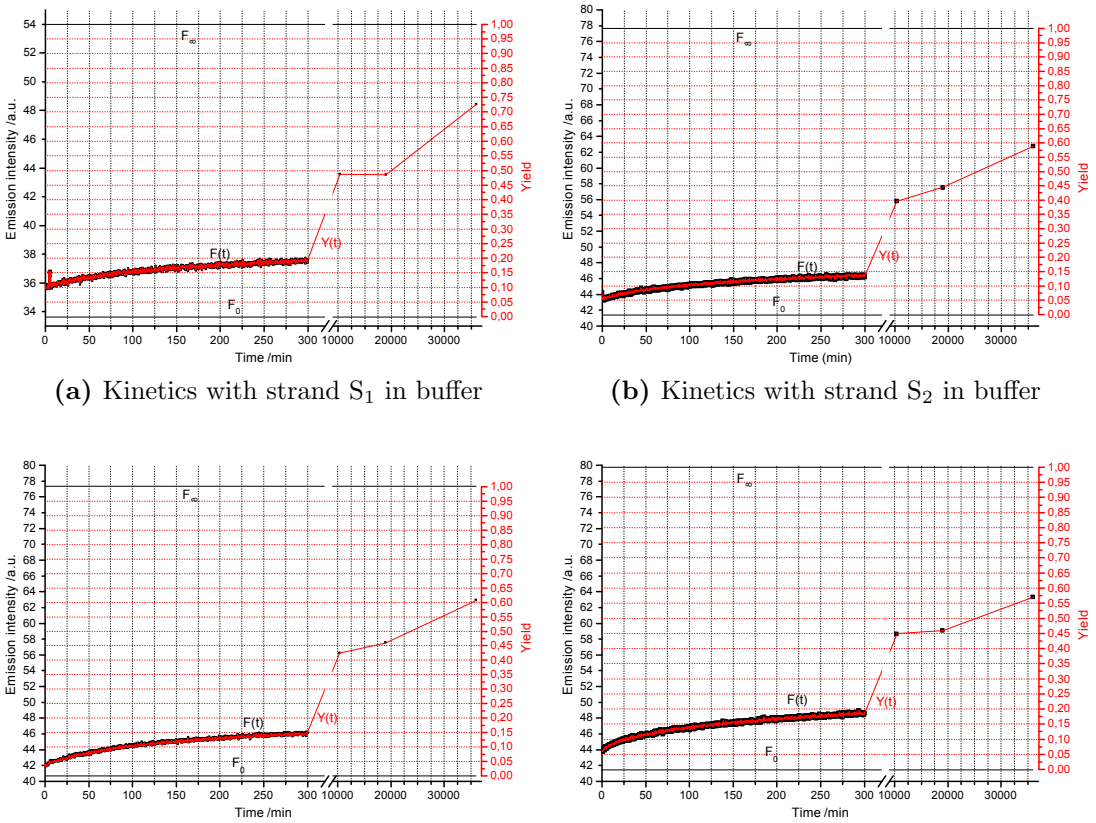

(a) Kinetics with strand S_1 in buffer

(b) Kinetics with strand S_2 in buffer

(c) Kinetics with strand S_4 in buffer

(d) Kinetics with strand S_5 in buffer

Figure 10.3: Kinetics traces of the four chosen strands in Na-phos. buffer. Yield is given in red. Reference samples are indicated by the F_∞- and F_0-labeled lines. See Table 10.4 for the corresponding inverted rate constants.

Table 10.4: Statistical summary for the curve fitting of kinetics in Na-phos. buffer. The coefficients of equation (2.8) are given with their respective with 95% confidence bounds within ()-brackets. See Figure 10.3for full traces.

Strands	F^*_∞ [a.u.]	ΔF [a.u.]	τ [s]	r^2	SSE	RMSE	$\text{Yield}_{300\text{min}}$ [%]
S_1	37.72 (37.68, 37.76)	1.971 (1.94, 2.003)	141 (134.1, 147.8)	0.9571	12.38	0.1019	19
S_2	46.67 (46.62, 46.71)	3.145 (3.108, 3.182)	141.8 (136.8, 146.8)	0.977	16.75	0.1183	14
S_4	46.41 (46.37, 46.45)	4.19 (4.157, 4.222)	129.2 (126, 132.3)	0.9871	17.26	0.12	15
S_5	48.94 (48.89, 48.99)	4.597 (4.556, 4.638)	132 (128.3, 135.7)	0.9836	26.2	0.1479	18

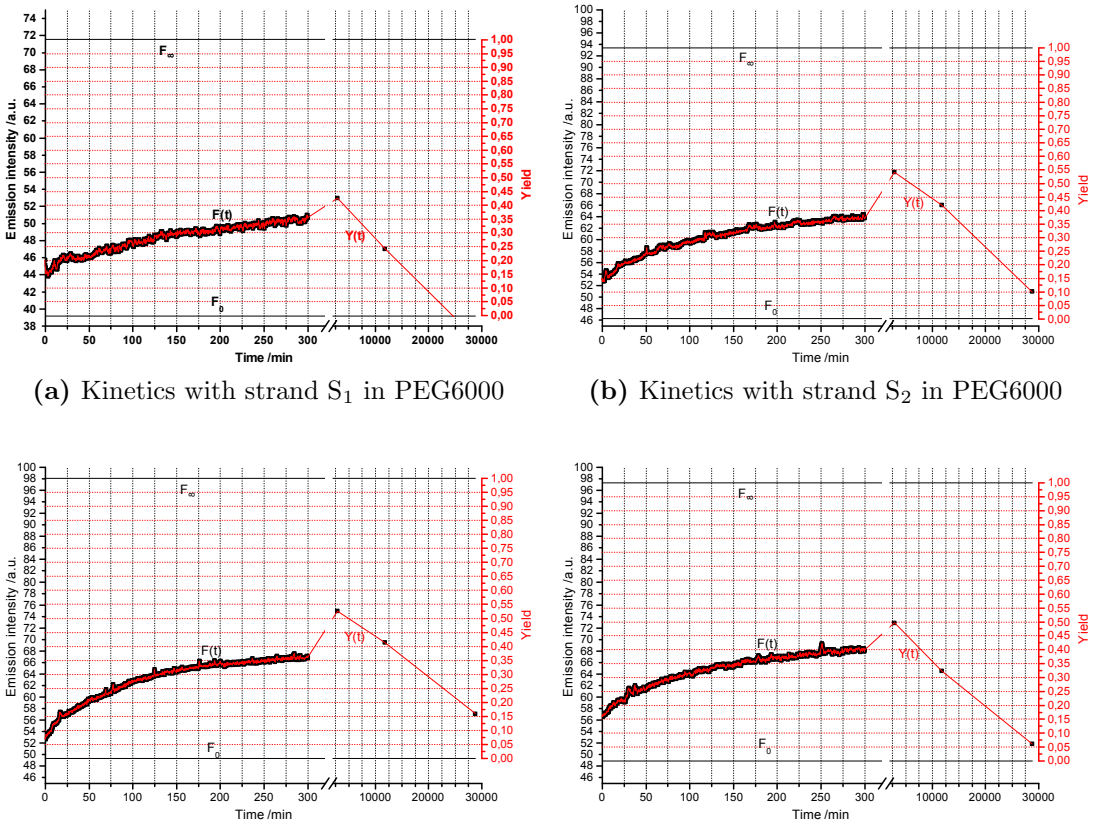

(a) Kinetics with strand S_1 in PEG6000

(b) Kinetics with strand S_2 in PEG6000

(c) Kinetics with strand S_4 in PEG6000

(d) Kinetics with strand S_5 in PEG6000

Figure 10.4: Kinetics traces of the four chosen strands in PEG6000. Reaction yields are given in red. Reference samples are indicated by the F_∞- and F_0-labeled lines. See Table 10.5 for the corresponding inverted rate constants.

Table 10.5: Statistical summary for the curve fitting of kinetics in PEG6000. The coefficients of equation (2.8) are given with their respective 95% confidence bounds within ()-brackets. See Figure 10.4 for full traces.

Strands	F^*_∞ [a.u.]	ΔF [a.u.]	τ [s]	r^2	SSE	RMSE	$\text{Yield}_{300\text{min}}$ [%]
S_1	51.69 (51.55, 51.83)	7.185 (7.072, 7.298)	173.8 (166.7, 181)	0.9776	71.2	0.2472	37
S_2	64.73 (64.64, 64.81)	11.21 (11.13, 11.28)	122.3 (119.8, 124.8)	0.9899	97.32	0.2854	38
S_4	67.35 (67.31, 67.4)	13.8 (13.75, 13.85)	93.9 (92.91, 94.9)	0.9961	55.85	0.2189	37
S_5	68.94 (68.87, 69.02)	11.62 (11.55, 11.68)	114.3 (112.3, 116.3)	0.9918	82.55	0.2662	40

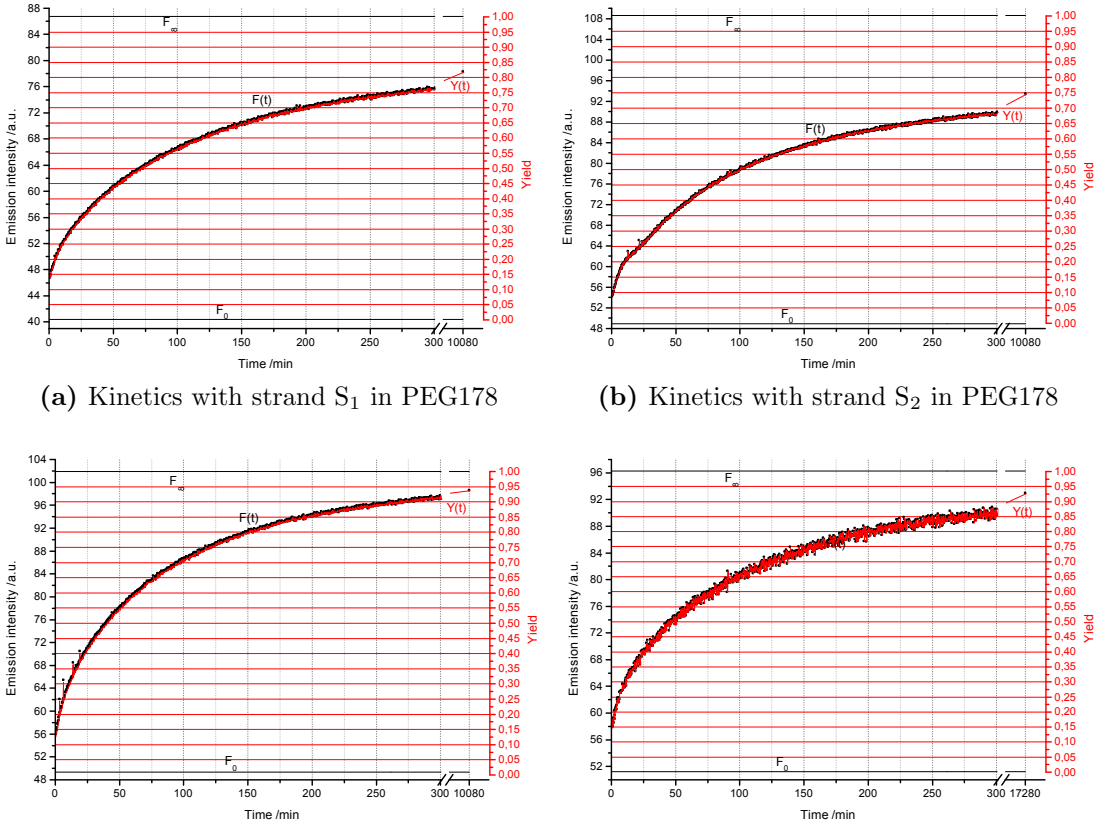

(a) Kinetics with strand S_1 in PEG178

(b) Kinetics with strand S_2 in PEG178

(c) Kinetics with strand S_4 in PEG178

(d) Kinetics with strand S_5 in PEG178

Figure 10.5: Kinetics traces of the four chosen strands in PEG178. Yield is given in red. Reference samples are indicated by the F_∞- and F_0-labeled lines. See Table 10.6 for the corresponding inverted rate constants.

Table 10.6: Statistical summary for the curve fitting of kinetics in PEG178. The coefficients of equation (2.8) are given their respective with 95% confidence bounds within ()-brackets. See Figure 10.5 for full traces.

Strands	F^*_∞ [a.u.]	ΔF [a.u.]	τ [s]	r^2	SSE	RMSE	$\text{Yield}_{300\text{min}}$ [%]
S_1	76.53 (76.45, 76.61)	27.21 (27.12, 27.3)	98.42 (97.47, 99.38)	0.9969	178.8	0.3878	77
S_2	90.75 (90.68, 90.82)	33.96 (33.89, 34.04)	96.41 (95.76, 97.06)	0.9985	136.3	0.3385	68
S_4	97.6 (97.51, 97.7)	37.43 (37.29, 37.56)	80.72 (79.94, 81.5)	0.9961	427.3	0.5982	92
S_5	90.61 (90.49, 90.74)	29.19 (29.05, 29.34)	92.24 (90.87, 93.61)	0.9922	535.4	0.6688	87

10.2 P2 C repressor project

Table 10.7: DNA strands DNA strands used in the P2 C repressor binding project with the production names of the strands and more convenient strand labels for easier reference. The position of the used base analogues tC^O and tC_{nitro} are indicated by **X** and **Y** in the DNA sequences, respectively. The calculated extinction coefficient at 260 nm are found in the rightmost column and the squences are 54 monomers long.

Strand name	Strand label	DNA sequences (54-mer)	ϵ_{260nm} [M^{-1} cm^{-1}]
B0399	P_1	5'-GTT TGA CAT GGT GTT TAG AT**X** TCA ATA GTA TTT CGT TTA GAT GTA GAT TGT TTA-3'	545 580
B0400	P_2	5'-GTT TGA CAT GGT GTT TAC ATC TCA ATA GTA TTT **X**GT TTA GAT GTA GAT TGT TTA-3'	545 580
B0401	P^*_{comp}	3'-CAA ACT GTA CCA CAA ATC TAG TGA TAT **Y**AT AAA GCA AAT CTA CAT CTA ACA AAT-5'	578 430
B0402	P_{unmod}	5'-GTT TGA CAT GGT GTT TAC ATC TCA ATA GTA TTT CGT TTA GAT GTA GAT TGT TTA-3'	542 340
B0403	P_{comp}	3'-CAA ACT GTA CCA CAA ATC TAG TGA TAT CAT AAA GCA AAT CTA CAT CTA ACA AAT-5'	575 460

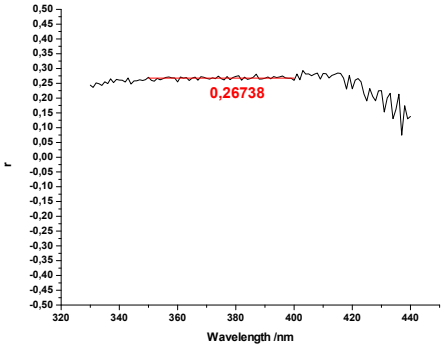

(a) $dsDNA_{P_2:P^*_{comp}}$

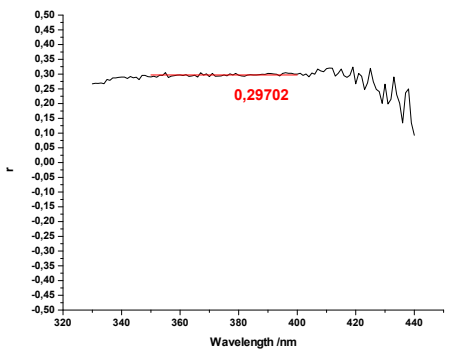

(b) P2 C sel. + $dsDNA_{P_2:P^*_{comp}}$

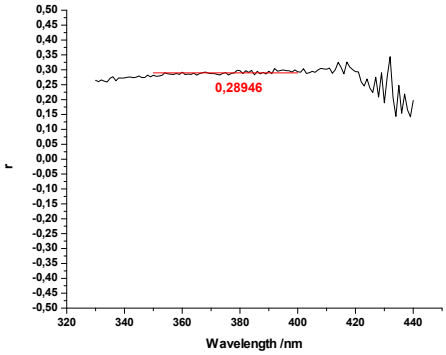

(c) P2 C wt + $dsDNA_{P_2:P^*_{comp}}$

Figure 10.6: Anisotropy measurements using tC^O in $dsDNA_{P_2:P^*_{comp}}$ using seleno and wt P2 C repressor. The red line represents the area of averaged anisotropy and the average value is stated in red.

Table 10.8: The full titration list for P2 C seleno protein 207.758 μM in to 1000 μL 2 μM $dsDNA_{P_2:P^*_{comp}}$. The last three values are fabricated for the purpose of helping fitting to the model. The extrapolated complex concentrations are derived through $\frac{1.984 \cdot 10^{-6} - 1.951 \cdot 10^{-6}}{2} + 1.984 \cdot 10^{-6} = 2.000 \cdot 10^{-6}$ M.

Tritration No.	Volume added [μL]	Total volume added [μL]	P2 C seleno dimer conc. [M]	P2 C seleno tetramer conc. [M	Complex conc. [M]
1	7.500e-07	7.500e-07	1.557e-07	7.785e-08	0.000e+00
2	7.500e-07	1.500e-06	3.112e-07	1.556e-07	2.123e-07
3	7.500e-07	2.250e-06	4.664e-07	2.332e-07	2.995e-07
4	7.500e-07	3.000e-06	6.214e-07	3.107e-07	3.602e-07
5	7.500e-07	3.750e-06	7.762e-07	3.881e-07	4.168e-07
6	1.500e-06	5.250e-06	1.085e-06	5.425e-07	4.688e-07
7	1.500e-06	6.750e-06	1.393e-06	6.965e-07	5.485e-07
8	1.500e-06	8.250e-06	1.700e-06	8.500e-07	6.302e-07
9	1.500e-06	9.750e-06	2.006e-06	1.003e-06	7.208e-07
10	1.500e-06	1.125e-05	2.311e-06	1.156e-06	7.957e-07
11	1.500e-06	1.275e-05	2.616e-06	1.308e-06	8.783e-07
12	1.500e-06	1.425e-05	2.919e-06	1.459e-06	9.593e-07
13	1.500e-06	1.575e-05	3.221e-06	1.611e-06	1.051e-06
14	1.500e-06	1.725e-05	3.523e-06	1.762e-06	1.114e-06
15	1.500e-06	1.875e-05	3.824e-06	1.912e-06	1.183e-06
16	1.500e-06	2.025e-05	4.124e-06	2.062e-06	1.271e-06
17	1.500e-06	2.175e-05	4.423e-06	2.211e-06	1.347e-06
18	1.500e-06	2.325e-05	4.721e-06	2.360e-06	1.424e-06
19	3.000e-06	2.625e-05	5.314e-06	2.657e-06	1.641e-06
20	3.000e-06	2.925e-05	5.904e-06	2.952e-06	1.750e-06
21	6.000e-06	3.525e-05	7.074e-06	3.537e-06	1.896e-06
22	6.000e-06	4.125e-05	8.231e-06	4.115e-06	1.951e-06
23	6.800e-06	4.805e-05	9.525e-06	4.763e-06	1.984e-06
-	-	-	-	7.000e-06	2.000e-06
-	-	-	-	9.000e-06	2.000e-06
-	-	-	-	12.00e-06	2.000e-06

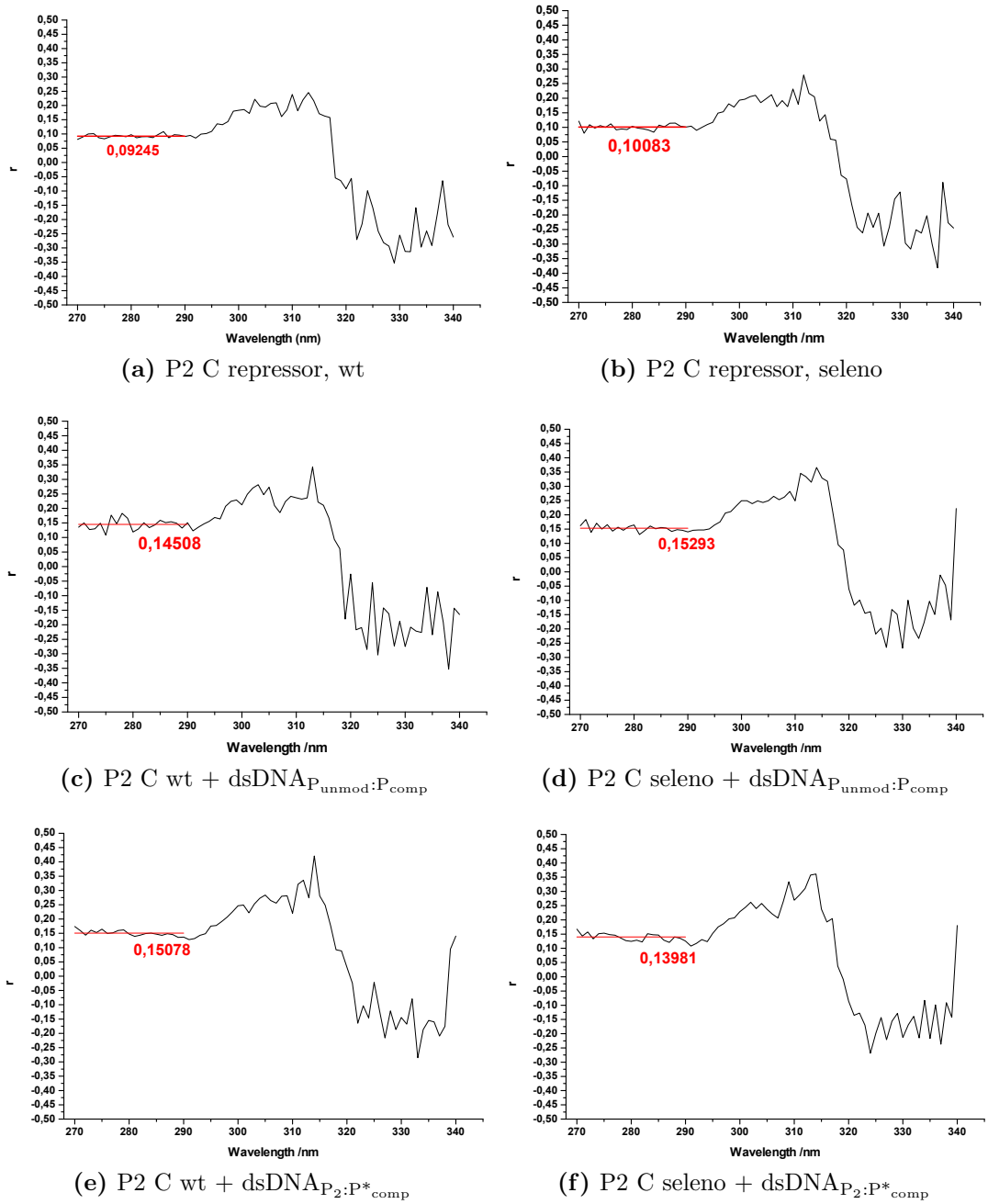

(a) P2 C repressor, wt

(b) P2 C repressor, seleno

(c) P2 C wt + dsDNA$_{\mathrm{P_{unmod}:P_{comp}}}$

(d) P2 C seleno + dsDNA$_{\mathrm{P_{unmod}:P_{comp}}}$

(e) P2 C wt + dsDNA$_{\mathrm{P_2:P^*_{comp}}}$

(f) P2 C seleno + dsDNA$_{\mathrm{P_2:P^*_{comp}}}$

Figure 10.7: Anisotropy measurements using tryptophan without duplex and in presence of modified and unmodified duplex. The red line represents the area of averaged anisotropy and the average value is stated in red. The three graphs in the left column represent P2 C repressor wt in the the three different cases and the right column correspondingly the P2 C repressor seleno.